Novel 3D Cubic Topology in Hybrid Lead Halides with a Symmetric Aromatic Triammonium Exhibiting Water Stability

Eugenia Vasileiadou, Imra Tajuddin, Michael de Siena, Vladislav Klepov, Mikaël Kepenekian, George Volonakis, Jacky Even, Lukasz Wojtas, Ioannis Spanopoulos, Xiuquan Zhou, et al.

Novel 3D Cubic Topology in Hybrid Lead Halides with a Symmetric Aromatic Triammonium Exhibiting Water Stability

Eugenia S. Vasileiadou, [1] Imra S. Tajuddin, [1] Michael C. De Siena, [1] Vladislav V. Klepov, [1] Mikaël Kepenekian, [2] George Volonakis, [2] Jacky Even, [3] Lukasz Wojtas, [4] Ioannis Spanopoulos, [4] Xiuquan Zhou, [5] Abishek K. Iyer, [1] Julie L. Fenton, [1] William R. Dichtel, [1] and Mercouri G. Kanatzidis [1,*]

[1] *Department of Chemistry, Northwestern University, Evanston, IL 60208, United States.*

[2] *Univ Rennes, ENSCR, CNRS, ISCR − UMR 6226, F-35000 Rennes, France.*

[3] *Univ Rennes, INSA Rennes, CNRS, Institut FOTON − UMR 6082, F-35000 Rennes, France*

[4] *Department of Chemistry, University of South Florida, Tampa, Florida 33620, United States*

[5] *Materials Science Division, Argonne National Laboratory, Lemont, Illinois 60439, USA*

Abstract:

The limitations of 3D perovskites are related to their narrow structural tunability of the organic cations and their moisture sensitivity. Herein, we report the new family of 3D cubic hybrid metal halides $(T\text{-}Et_6)_3Pb_{11}X_{31}$ (X=I, Br), where T is 1,3,5-tris-(4-aminophenyl)benzene. The materials are synthesized through an *in-situ* N-alkylation of T and an efficient one-step solvothermal reaction containing ethanol, initiating a tunable synthetic avenue for the acquisition of structurally complex hybrid halides with luminophores. $(T\text{-}Et_6)_3Pb_{11}X_{31}$ consists of an unprecedented $Ia\bar{3}$ framework of $[Pb_{11}X_{31}]^{9-}$ 1D chains embedded with $(T\text{-}Et_6)^{3+}$ cations affording an overall 3D topology. The constituent $[Pb_{11}X_{31}]^{9-}$ chains include exclusively octahedral lead halide units with clusters of face- and edge-sharing connectivity, giving rise to weak broad emission centered at ~660 nm observed at 78K. $(T\text{-}Et_6)_3Pb_{11}I_{31}$ demonstrates water stability for at least 7 days. Synthesis through ambient-pressure results in tunable structural variations of 0D structures rendering $T_7Pb_3Br_{27}{\cdot}DMF$ and $T_2Sn_3Br_{18}{\cdot}4H_2O{\cdot}0.5Br_2$, both of which feature blue PL emission at room temperature.

Introduction:

3D hybrid halide perovskites have become a prominent class of semiconductor research due to their attractive, tunable optoelectronic properties and low-temperature solution syntheses-processibility, which allow for a broad range of optoelectronic applications such as solar cells,[1-9] light emission,[10-12] radiation detection[13-17] and lasing.[18-19] The 3D halide perovskite structure has the general formula AMX_3, composed of a 3D network of corner-sharing metal halide $[MX_6]^{4-}$ octahedra with the A-site cation occupying the center of the cuboctahedral cavities. A is one of the monovalent cations: Cs^+, $CH_3NH_3^+$ (MA^+), $HC(NH_2)_2^+$ (FA^+) or recently $CH_3NH_2NH_2^+$ [20-21] and $(CH_2)_2NH_2^+$,[22] M is a divalent metal (Ge^{2+}, Sn^{2+}, Pb^{2+})[23] and X is a halide (Cl^-, Br^-, or I^-). [24-25] Consequently, the compositional tailoring of 3D halide perovskites is limited to small, hydrophilic organic cations that render the material to being moisture sensitive.[26-32] Lastly, 3D halide perovskites crystallize in high-symmetry cubic space groups with phase transitions affording the tetragonal and orthorhombic polymorphs.[33-36]

Recently, a new class of 3D metal halide compounds have been investigated that incorporate diammonium cations larger than the A-site cation, affording a 3D network of both corner-sharing and edge-sharing connecting of $[MX_6]^{4-}$ octahedra.[37-45] These compounds are referred to as perovskitoids as they display multiple attributes similar to 3D perovskites due to the corner-sharing $(M_2X_2X_{8/2})_\infty^{2-}$ frameworks, however they are lower in symmetry adapting mainly orthorhombic or monoclinic space groups.[38-42] Beyond the 3D perovskitoids, there is a meager amount of other octahedral structural motifs of 3D hybrid lead halide compounds reported with no design principles on how to rationally expand this phase space. Specifically, $(Et_2NHC_6H_4\text{-}CH_2C_6H_4NHEt_2)_{2n}(Pb_7I_{18})_n \cdot 4nH_2O$ is an open framework structure exhibiting photochromism that belongs to the monoclinic $C2/c$ space group, which displays edge-sharing $[PbI_6]^{4-}$ octahedra interlinking at a crystallographic inversion center to form incomplete cubane chains along the [110] or $[1\bar{1}0]$ direction.[46] $(H_2DABCO)(Pb_2Cl_6)$ and $(H_3O)(Et_2\text{-}DABCO)_8(Pb_{21}Cl_{59})$ (DABCO : ¼ 1,4-diazabicyclo[2.2.2]-octane) are 3D structures belonging to the tetragonal space group $P4_32_12$ and monoclinic space group $P2_1/c$ respectively with corner-sharing $[PbCl_6]^{4-}$ octahedra forming nodes that demonstrate a high color rendering index of white-light emission.[47] Finally, $(HOOC(CH_2)_3NH_3)PbI_3$ is 3D structure displaying thermochromism that belongs to the orthorhombic space group *I*mma, which presents an inorganic unit of edge-sharing and face-sharing $[PbI_6]^{4-}$ octahedra that ultimately form a diamond-like 3D framwork.[48]

The 3D hybrid halide perovskite structure can be dimensionally reduced to layers of 2D structure,[29, 43, 49-55] chains of 1D structure[56-60] or 0D clusters of $[MX_6]^{4-}$ octahedra[61-64] through the incorporation of diverse organic cations. These organic cations are larger than the aforementioned A-site cations, permitting a vast compositional space of structural tunability for the synthesis of new hybrid halide materials for optoelectronic and technological applications [52-53, 65-76] Despite the expandable phase space, the reported bulk, hybrid metal halide perovskite-related frameworks mainly features aliphatic or aromatic organic cations that are not optically active and do not contribute to the luminescent properties of the hybrid material.[20-21, 49, 51, 60, 77-86] Whereas the incorporation of organic luminophores is comparatively a much more narrow phase space with insufficient structural design principles to guide the rational synthetic design of functional hybrid materials. [66, 68, 87-92] In order to establish greater structural complexity in luminsecent hybrid metal halides while significantly enhancing the moisture stability of the resultant compounds, it is desirable to template sophisticated hybrid halide compounds with optically active organic cations.[66, 89-90, 92-94] Thus far, only a handful of low dimensional water-stable hybrid halide perovskites have been reported such as (1,8-octyldiammonium)Sn_2I_6 that is water stable for at least 15 hrs,[69] $[Pb_2Cl_2]^{2+}[^{-}O_2C(CH_2)_4CO_2^{-}]$ that is water stable for 24 hrs,[95] [N-methyldabconium]PbI_3 that is water stable for 1 month [96] and (4,4'-ethylenedipyridinium)Pb_2Br_6 that is water stable for 180 days.[93]

Herein, we demonstrate that hybrid metal halides can acquire unusually high structurally complexity and cubic symmetry by incorporating the symmetric triamine luminophore 1,3,5-tris-(4-aminophenyl)benzene, hereby symbolized T. We establish a new class of water-stable hybrid metal halide compounds with the T triammonium cation, where T is a π-electron rich molecule with a C_3-symmetric propeller shape and inherent optical and high dielectric nature.[97] Through a one-step solvothermal synthesis in ethanol, the T cation *in-situ* ethylates all three amine sites to give the T-Et_6 trication, producing the cubic $(T\text{-}Et_6)_3Pb_{11}X_{31}$ (X=I, Br) compounds. The provided synthetic preparation provides a viable avenue to fine tune the organic luminophore and the inorganic lattice in the solid-state, yielding new hybrid structural motifs. $(T\text{-}Et_6)_3Pb_{11}X_{31}$ (X=I, Br) present an unprecedent framework of $[Pb_{11}X_{31}]^{9-}$ 1D chains inlayed with $(T\text{-}Et_6)^{3+}$ cations that build altogether a 3D topology. The electronic structure of $(T\text{-}Et_6)_3Pb_{11}I_{31}$ shows the density of states' final relocalization resulting in essentially flat bands within the VB and CB. $(T\text{-}Et_6)_3Pb_{11}I_{31}$ presents an absorption edge at 1.9 eV with weak broad emission centered at ~660 nm at 78K.

Through ambient-pressure solution synthesis, adjustable structural variations of 0D structures with T^{3+} cations are acquired, yielding compounds $T_7Pb_3Br_{27}$·DMF and $T_2Sn_3Br_{18}$·$4H_2O$·$0.5Br_2$. Owing to the incorporation of T^{3+} cations, $T_7Pb_3Br_{27}$·DMF and $T_2Sn_3Br_{18}$·$4H_2O$·$0.5Br_2$ feature blue PL emission at room temperature. All four novel compounds exhibit moisture-stability. $(T\text{-}Et_6)_3Pb_{11}I_{31}$ is the only known 3D hybrid lead halide with water stability to our knowledge. Our work establishes the synthetic design of sophisticated and water-stable hybrid semiconductors with high-symmetry luminophores that render unique structural motifs, optoelectronic features, and moisture stability.

Experimental Section

All starting materials for synthesis were purchased commercially and were used without further purification. $Pb(CH_3COO)_2·3H_2O$ (99.9%), NaI, NaBr, Ethyl alcohol, 1,3,5-Tris(4-aminophenyl)benzene, hydroiodic acid (HI) (57 wt % in H_2O, distilled, stabilized, 99.95%), hydrobromic acid (ACS reagent, 48 wt % in H_2O) and hypophosphorous acid solution (50 wt % in H_2O) were purchased from Sigma-Aldrich and used as received.

Synthesis of $(T\text{-}Et_6)_3Pb_{11}I_{31}$: Lead acetate trihydrate (0.2 mmol, 75.9 mg), 1,3,5-Tris(4-aminophenyl)benzene (0.06 mmol, 20 mg), and NaI (0.2 mmol, 30 mg) were weighed and placed in a teflon chamber. 0.25 mL of HI and 5 mL of anhydrous ethanol were added, after which the teflon chamber was sealed inside a stainless-steel chamber. The reaction mixture was heated at 160°C for 6 days and cooled for 24 hours. The teflon chamber was opened and found to have precipitated brown-yellow rod-like crystals.

Synthesis of $(T\text{-}Et_6)_3Pb_{11}Br_{31}$: Lead acetate trihydrate (0.2 mmol, 75.9 mg), 1,3,5-Tris(4-aminophenyl)benzene (0.06 mmol, 20 mg), and NaBr (0.2 mmol, 20.5 mg) were weighed and placed in a teflon chamber. 0.25 mL of HBr and 5 mL of anhydrous ethanol were added, after which the teflon chamber was sealed inside a stainless-steel chamber. The reaction mixture was heated at 160°C for 6 days and then cooled for 24 hours. The teflon chamber was opened and found to have precipitated orange block crystals along with yellow needle crystals.

Synthesis of T·3HBr: 1,3,5-Tris(4-aminophenyl)benzene (0.15 mmol, 50 mg) was added to 2 mL HBr and heated at 200°C. A clear yellow solution was formed, and the solution became white over a continual heating period. The reaction mixture was allowed to cool to room temperature,

afterwards the cooled mixture was vacuum filtered and dried under vacuum. The solid yield after drying was 57.2 mg.

Synthesis of $T_7[PbBr_6]_3Br_9$•DMF : PbO (1 mmol, 223 mg) was dissolved in 5 mL HBr by heating to boiling at 200°C under constant magnetic stirring until a clear solution was obtained. 1,3,5-Tris(4-aminophenyl)benzene (0.06 mmol, 20 mg) and 1 mL DMF were added to the reaction mixture. A cloudy white precipitate crashed out, which turned pale cloudy pink upon continuous heating. The hotplate and stirring were then turned off, and the reaction solution was cooled to room temperature; Clear, thin needle crystals precipitated from the mixture. The reaction mixture was vacuum filtered and dried under vacuum.

Synthesis of $T_2Sn_3Br_{18}·4H_2O·0.5Br_2$: $SnCl_2·2H_2O$ (1 mmol, 225.64 mg) was dissolved in a mixture of 4 mL HBr and 2 mL H_3PO_2 by heating to boiling at 200°C under constant magnetic stirring until a clear solution was obtained. 1,3,5-Tris(4-aminophenyl)benzene (0.1 mmol, 35 mg) was added to the reaction mixture. A cloudy yellow precipitate crashed out. The hotplate and stirring were then turned off, and the reaction solution was cooled to room temperature; Tiny yellow-clear needle crystals precipitated from the mixture. The reaction mixture was vacuum filtered and dried under vacuum.

Results and Discussion:

Synthetic Aspects:

Attempts to synthesize various dimensionality (1D, 2D or 3D) lead halide compounds incorporating the triamine molecule, T, through the classic solution synthesis at ambient-pressure by employing hydrohalic acid would not yield any crystalline product. The solubility of T in HX solvent is limited so DMF was added to the synthesis under heating and stirring. In the case of the HI/DMF solution, yellow crystals of $DMAPbI_3$ (DMA: dimethylamine) form as a result of the hydrolysis of DMF in heated hydroiodic acid that is known in the literature.[98-99] In the case of the HBr/DMF solution, a new colorless compound incorporating T is formed with formula $T_7Pb_3Br_{27}·DMF$ that has a 0D structure as verified by single crystal X-ray diffraction (See *Crystal Structure* Section below). Lastly, in order to obtain other hybrid metal halide compounds incorporating T, solution synthesis at ambient pressure was undertaken using $SnCl_2·2H_2O$ and T in a HBr/H_3PO_2 solution that yielded light-yellow needle crystals of the 0D structure

$T_2Sn_3Br_{18}\cdot 4H_2O\cdot 0.5Br_2$. Details of the syntheses of $T_7Pb_3Br_{27}\cdot DMF$ and $T_2Sn_3Br_{18}$ are in the *Experimental Section.*

Brown-yellow crystals of $(T\text{-}Et_6)_3Pb_{11}I_{31}$ and orange-yellow crystals of $(T\text{-}Et_6)_3Pb_{11}Br_{31}$ (**Figure 1D and Figure 1E**) were successfully obtained from solvothermal treatment of T, $Pb(CH_3COO_2)_2\cdot 3H_2O$ and NaX (X=I, Br) in ethanol and HX (X=I, Br) at 160°C for 6 days. Details of the exact syntheses are in the *Experimental Section.* $Pb(CH_3COO_2)_2\cdot 3H_2O$ is the source of Pb^{2+} and NaX (X=I, Br) is the source of X^- halide anion in the syntheses. Hydroiodic acid (HI) and hydrobromic acid (HBr) are employed respectively to protonate the triamine molecule T in a ratio 20:1 solvent to HX, overall leading to the creation of an acidic environment for the solvothermal synthesis. As a result of the acidic synthetic conditions,[73] the triamine molecule T undergoes a one-step, *in situ* N-diethylation reaction with the excess ethanol solvent to form the N-hexa-ethylated species $(T\text{-}Et_6)^{3+}$ (**Scheme 1**). It is noteworthy that the solvothermal conditions along with the obtained N-hexa-ethylated species $(T\text{-}Et_6)^{3+}$ serve a critical role in the self-assembly of the acquired $(T\text{-}Et_6)_3Pb_{11}X_{31}$ (X=I, Br) products. Single crystal X-ray diffraction (**Figure 1**) and NMR spectroscopy (**Figure S17**) verify the existence of the $(T\text{-}Et_6)^{3+}$ molecule in compounds $(T\text{-}Et_6)_3Pb_{11}X_{31}$ (X=I, Br). The reproducibility of the synthesis of $(T\text{-}Et_6)_3Pb_{11}X_{31}$ (X=I, Br) was confirmed where after multiple repetitions of the solvothermal reactions, all the experimental powder X-ray diffraction (PXRD) patterns match the simulated pattern of $(T\text{-}Et_6)_3Pb_{11}I_{31}$ (**Figure S6**). Therefore, the solvothermal synthetic technique can provide efficient routes to hybrid metal halide compounds that significantly enriches the phase space of perovskite-related compounds beyond the limited currently known structure types.

Powder X-ray diffraction verified the acquisition of the titled compounds with a small impurity phase present at $2\theta=9°$ that could not be identified (**Figure S1** and **Figure S2**). Under the microscope, there is no apparent secondary phase that can be identified for the case of $(T\text{-}Et_6)_3Pb_{11}I_{31}$. The synthesis of $(T\text{-}Et_6)_3Pb_{11}Br_{31}$ yielded a distinct secondary phase of yellow needles. Single crystal X-ray diffraction analysis showed this phase is a cubic 3D assembly of lead halide chains templated by the $T\text{-}Et_6$ trications.

Description of Crystal Structures:

Compounds with 3D Cubic Topology

$(T\text{-}Et_6)_3Pb_{11}X_{31}$ (X=I, Br) represent a unique structure type and new class of hybrid lead halide compounds with 3D cubic topology formed from purely octahedral units of 1D lead halide chains (**Figure 1**). The 3D topology of $(T\text{-}Et_6)_3Pb_{11}X_{31}$ (X=I, Br) consists of the complex $[Pb_{11}X_{31}]^{9-}$ 1D chain that serves as the building block of the inorganic framework. The $[Pb_{11}X_{31}]^{9-}$ chain features 5 consecutive face-sharing $[PbX_6]^{4-}$ units connected to a cluster of 6 edge-sharing $[PbX_6]^{4-}$ units (**Figure 1B**). The $[Pb_{11}X_{31}]^{9-}$ chains do not bond to each other but instead weave a 3D tangled network that can be analogized to fabric weaves (**Figure 1A**). The 3D topology in $(T\text{-}Et_6)_3Pb_{11}X_{31}$ (X=I, Br) has cubic symmetry ($Ia\bar{3}$ space group in this case) that is unique. To our knowledge, there are no reports of hybrid lead halide compounds with high-symmetry cubic space groups, besides the well-known family of 3D hybrid lead halide perovskites, which belong to the cubic space group $Pm\bar{3}m$ and feature purely 3D corner-sharing motifs of $[PbI_6]^{4-}$octahedra.[100] For this new structure type of $(T\text{-}Et_6)_3Pb_{11}X_{31}$ (X=I, Br), the high cubic symmetry is directed by the novel organic molecule $(T\text{-}Et_6)^{3+}$ and their three-fold symmetry (**Scheme 1**). It is important to make a distinction between the dimensionality of structural units and overall topology of the structure. $(T\text{-}Et_6)_3Pb_{11}X_{31}$ (X=I, Br) are hybrid compounds consisting of secondary units of organic and inorganic chains. The organic framework of $(T\text{-}Et_6)^{3+}$ cations embedded within the homogeneous cubic packing of the inorganic $[Pb_{11}X_{31}]^{9-}$ 1D chains produces the resultant, hybrid compounds $(T\text{-}Et_6)_3Pb_{11}X_{31}$ (X=I, Br) that form an overall 3D topology. The topology of the structure without chain overlaps can only be represented in 3D space, thus this crystal structure has 3D (but 1-periodic) topology based on 1D structural units.

The triamine-based molecules' high symmetry and greater ability for electrostatic interactions leads to the unique, high symmetry self-assembly of the result hybrid organic-inorganic network. The four $[Pb_{11}X_{31}]^{9-}$ chains run along the [1,0,0], [0,1,0], [0,0,1] and [1,1,1] directions and are all related to each other by symmetry. O'Keeffe et al., have developed an analytical description of homogenous packings of cubic cylinder motifs,[101-102] where the term "cylinder packing" refers to the infinite packings of 1D cylinder motifs in which each cylinder relates to all the others by crystallographic symmetry operations. The $(T\text{-}Et_6)_3Pb_{11}X_{31}$ structures belong to the non-bundle <111> cylinder packings[102] (Type No.1) with 4 cylinder chains $[Pb_{11}X_{31}]^{9-}$ within the unit cell.[102] The 4 cylinder chains can be described based on the body diagonal cylinder lengths that fall within one cubic unit cell, where along the [111] direction in the $(T\text{-}Et_6)_3Pb_{11}X_{31}$ structures there are one full $[Pb_{11}X_{31}]^{9-}$ chain and 6 halves chains resulting in 4

chains altogether. Furthermore, the symmetry in O'Keeffe et al., [102] is an idealized (highest) symmetry for the non-bundle <111> cylinder packings that can be lowered in real chemical systems. As a result, the $(T\text{-}Et_6)_3Pb_{11}X_{31}$ structures that crystallize in the $Ia\bar{3}$ space group correspond to the Type 1 <111> cylinder packing with idealized $Ia\overline{3d}$ space group[102].

On the other hand, from a symmetry viewpoint, the $Ia\bar{3}$ cubic space group (T_h) corresponds to a slightly lower symmetry than the $Pm\bar{3}m$ space group (O_h) lacking essentially four-fold axes. Nevertheless, the crystallographic structure exhibits three-fold symmetry axes, as this symmetry operation finds its origin in each sub-network of 1D $[Pb_{11}X_{31}]^{9-}$ lead halide chains. Indeed, the sub-network of 1D lead halide chains is related to the trigonal R space group, where the triamine-based molecules maintain this symmetry. The electronic properties of the whole structure may be indeed understood by considering firstly those of each sub-network of 1D lead halides, and then the coupling between the four $[Pb_{11}X_{31}]^{9-}$ chains in the composite structure (vide infra, see **S.I.** Section 3.5 *Electronic Calculations*).

Significantly, halide atoms I5 and Br5 in the structure have a very rare octahedral coordination where they are sitting in the center of a Pb-X fragment with a NaCl-type motif (**Figure 1C**). Of the other known examples of an iodine atom in octahedral coordination within a hybrid lead halide $[Pb_6I_{19}]$ cluster is the example with viologen molecules[103-104] of 1D structures such as $(C_{12}H_{14}N_2)Pb_2I_6$ where $C_{12}H_{14}N_2$ is methylviologen and the Pb^{2+} features both octahedral and trigonal prismatic coordination within the inorganic framework[103], as well as $(C_4H_9N)_8Pb_{18}I_{44}$[105]. Overall, between the two analogues compounds $(T\text{-}Et_6)_3Pb_{11}X_{31}$ (X=I, Br) bromide compound $(T\text{-}Et_6)_3Pb_{11}Br_{31}$ unit cell dimensions are 0.792 Å smaller and its volume is 2706.39 $Å^3$ smaller than $(T\text{-}Et_6)_3Pb_{11}I_{31}$ (**Table 1**). Additionally, there is notable elongation of the Pb-X bond lengths within the $[Pb_{11}X_{31}]^{9-}$ framework with an average bond length of Pb-I equal to 3.213 Å and even more dramatic elongation for the bromide compound with an average bond length of Pb-Br equal to 3.086 Å (**Table 2**). In comparison the average Pb-X length in 3D halide perovskites is around 3.15 Å for Pb-I bonds and 2.97 Å for Pb-Br bonds.[24]

Viewing the crystal structure $(T\text{-}Et_6)_3Pb_{11}I_{31}$ along the [100] direction (**Figure 2A**) demonstrates how the $[Pb_{11}X_{31}]^{9-}$ 1D chain intercross at various orientations, where the $[Pb_{11}I_{31}]^{9-}$ chains shaded with the same color are directed in the same orientation. The contact distance between the $[Pb_{11}I_{31}]^{9-}$ chains is 4.486 Å for $(T\text{-}Et_6)_3Pb_{11}I_{31}$ (**Table 2**), as shown in **Figure 2B**. The

molecular three-fold axis of the organic cations $(T\text{-}Et_6)^{3+}$ coincides with the three-fold axis of the unit cell. The shortest nitrogen-iodine distance in $(T\text{-}Et_6)Pb_{11}I_{31}$ is N3-I2 = 3.701Å implying a significant I···H hydrogen bonding. The closest contact of a nitrogen atom on the $(T\text{-}Et_6)^{3+}$ molecule to an aromatic carbon atom from an adjacent $(T\text{-}Et_6)^{3+}$ molecule is 4.803 Å. The closest distance of aromatic carbon atoms from adjacent $(T\text{-}Et_6)^{3+}$ cations 5.623 Å, indicating that π-π stacking is not apparent. On the other hand, for the $(T\text{-}Et_6)_3Pb_{11}Br_{31}$ compound, the contact distance between the $[Pb_{11}Br_{31}]^{9-}$ chains is 4.852 Å, a slightly larger distance than in the iodide analog despite the smaller unit cell dimension and volume of $(T\text{-}Et_6)_3Pb_{11}Br_{31}$ (**Table 2**). However, the nitrogen-bromide distance is smaller with N1-Br3 = 3.488 Å consistent with significant Br···H hydrogen bonding, and the closest contact of a nitrogen atom on the $(T\text{-}Et_6)^{3+}$ molecule to an aromatic carbon atom from an adjacent $(T\text{-}Et_6)^{3+}$ molecule is 1.596 Å. Due to the cubic symmetry, the contact angle between $[Pb_{11}X_{31}]^{9-}$ chains in both $(T\text{-}Et_6)_3Pb_{11}I_{31}$ and $(T\text{-}Et_6)_3Pb_{11}Br_{31}$ are identical at 70.53°.

Reversible-cycle differential scanning calorimetry (DSC) was performed on $(T\text{-}Et_6)_3Pb_{11}I_{31}$ crystal sample in the temperature range of -50ºC to 120ºC to identify any phase transitions. Temperature-dependent phase transitions are a frequent phenomenon in hybrid halide perovskites. From the DSC measurements, it was possible to identify a reversible-phase transition for $(T\text{-}Et_6)_3Pb_{11}I_{31}$ that presents an endothermic peak at -24°C (**Figure S8**). The sharp shape of the transition peaks presents the characteristic of a first-order transition.

Compounds with 0D Topology

The crystal structures of 0D compounds $T_7Pb_3Br_{27}{\cdot}DMF$ and $T_2Sn_3Br_{18}{\cdot}4H_2O{\cdot}0.5Br_2$ containing the T molecule were obtained from the solution synthesis on a hotplate at ambient pressure (**Figure 3**). Single crystal X-ray diffraction demonstrates that $T_7Pb_3Br_{27}{\cdot}DMF$ is essentially a double salt with T^{3+} cations between the isolated $[PbBr_6]^{4-}$ octahedra and with bromine atoms coordinated to DMF molecules such as the chemical formula can also be described as $T_7[PbBr_6]_3{\cdot}[Br]_9{\cdot}DMF$. The PXRD of the experimental pattern of the $T_7Pb_3Br_{27}{\cdot}DMF$ crystals matches the simulated pattern derived from the single crystal X-ray structure (**Figure S4**). Furthermore, $T_2Sn_3Br_{18}{\cdot}4H_2O{\cdot}0.5Br_2$ is also a 0D structure featuring isolated tin bromide octahedra with T^{3+} cations between with Sn^{4+} oxidation state. Additionally, in $T_2Sn_3Br_{18}{\cdot}4H_2O{\cdot}0.5Br_2$, the bromide atoms of the $[SnBr_6]^{2-}$ octahedra are coordinated to water molecules and the Br_2 moiety

forms hydrogen bonds with the ammonium groups of the T^{3+} cations. The experimental PXRD pattern of $T_2Sn_3Br_{18}{\cdot}4H_2O{\cdot}0.5Br_2$ crystals matches the simulated pattern, verifying the phase acquisition (**Figure S5**). Interestingly, higher dimensionality compounds than 0D could not be acquired through the solution synthesis at ambient-pressure, suggesting that the bonding of such large hydrocarbon amines have weak electrostatic interaction with the lead-halide frameworks, despite the beneficial attributes of π-conjugation, aromaticity, and polyamine groups. In the case of the solvothermal synthesis, the additive effect of high vapor pressure which results in the full ethylation of the amino groups on the T molecule proves to be critical in acquiring the 3D compounds $(T\text{-}Et_6)_3Pb_{11}X_{31}$ (X=I, Br).

Stability:

A limiting factor in the development of 3D hybrid halide perovskite devices for optoelectronic applications is their long-term stability under operating conditions. Introducing more hydrophobic and bulky organic cations endows enhanced stability in the resultant lower-dimensional congeners of 2D perovskites and even lower dimensional 1D- and 0D-related frameworks.[29, 32, 52-53] Thus, there is broad interest in hybrid lead halide compounds with moisture stability. The $(T\text{-}Et_6)_3Pb_{11}X_{31}$ (X=I, Br) with its bulky, hydrophobic $(T\text{-}Et_6)^{3+}$ cations and 3D topology provides a rare example of a water stable system. Crystals of $(T\text{-}Et_6)_3Pb_{11}I_{31}$ retain their structural integrity after being exposed to ambient air in the dark for three months, as it can be seen in the PXRDs of **Figure 4A.** Moreover, $(T\text{-}Et_6)_3Pb_{11}I_{31}$ crystals were added to a vial with water and after 7 days the collected PXRD pattern showed no structural decomposition (**Figure 4B**). Moreover, the 0D compounds $T_7[PbBr_6]_3{\cdot}$ $[Br]_9{\cdot}DMF$ and $T_2Sn_3Br_{18}{\cdot}4H_2O{\cdot}0.5Br_2$ also maintain their structural integrity upon prolonged exposure to ambient air upon PXRD observation.

Optical Properties:

The optical bandgaps of the synthesized compounds are extrapolated from the absorption onset based on the optical absorption spectra shown in **Figure 5** and **Figure S11**, which were measured at room temperature. They are estimated by extrapolating from the absorption edges, a slope perpendicular to the x axis. Compound $(T\text{-}Et_6)_3Pb_{11}I_{31}$ exhibits one absorption edge with estimated bandgap 1.72 eV. The protonated triamine T·3HBr feature two absorption edges with an estimated bandgap 2.24 eV. The 0D compound $T_7Pb_3Br_{27}{\cdot}DMF$ displays three absorption edges

with an estimated bandgap 2.75 eV. $T_2Sn_3Br_{18}{\cdot}4H_2O{\cdot}0.5Br_2$ displays two absorption edges with estimated bandgap 2.40 eV. Summary of the optical properties of the materials are outlined in **Table 3**. Weak absorption may be due to the observed absorption being dominated not by a band edge transition but rather it is highly convoluted owing to the presence of the organic component. The absorption spectrum of the protonated amine is presented in **Figure 5** and this spectrum shows considerable spectral overlap with the metal halide compounds presented here, complicating an assignment of peaks with the current data. To further our understanding of this new structural family of hybrid metal halides will require more detailed investigations of their optical properties in a separate study.

The photoluminescence (PL) emission spectra of the 3D triamine lead halides (**Figure 6**) and 0D triamine lead halide compounds (**Figure 7**) were collected at room temperature. The photoluminescence properties of the pure triamine molecule T (**Figure S9 A,B**) and the protonated triamine T·3HBr species (**Figure S9 C,D**) are given in the **S.I.** The protonated triamine T·3HBr species shows a red-shift in the emission properties as compared to the T species consistent with what is observed in the absorption data (**Figure S9**). Further details on the optical properties of amino substituted triphenylbenzene derivatives with a 3-fold symmetry (like ours) has been reported elsewhere.[106]

Compound $(T\text{-}Et_6)_3Pb_{11}I_{31}$ did not display any measurable photoluminescence at room temperature; however, emission was observed at 78 K (**Figure 6A**). Two peaks are observed at this temperature, a strong narrow emission centered at 750 nm, and a weak broad emission at higher energy centered at ~660 nm, thus indicating a more complex PL mechanism with some of this luminescence arising from traps. Further assignment of this high-energy emission band is beyond the scope of this work and a more detailed study on the temperature-dependent optical properties of this compound is required. The narrow, low energy emission peak displays slow biexponential recovery kinetics with a fast 51 ns and a slow 1.3 μs component (**Figure 6B**). The observed emission at 750 nm at low temperature is found well below the estimated optical bandgap of the material (1.72 eV); however, we note that the band gap is measured at RT whereas the emission is measured at 78 K.

The $T_7[PbBr_6]_3{\cdot}[Br]_9{\cdot}$DMF compound (**Figure 7**) displays blue emission at 404 nm when excited at 330 nm. When excited at 405 nm, the compound displays broad emission centered at ~520 nm. These two bands are assigned to different origins with the high-energy narrow band

assigned to localized $[PbBr_6]^{4-}$-based emission and the low energy broad band to T-based emission. Furthermore, photoluminescence excitation spectra support that these two luminescence features have distinct origins. The excitation spectrum monitoring the 404 nm-centered emission shows two strong bands at ~290 and ~350 nm that are consistent with the reported electronic transitions in isolated $[PbBr_6]^{4-}$ octahedra in the 0D Cs_4PbBr_6 material further supporting our assignment of this emission.[107-108] The excitation spectrum monitoring the 520 nm-centered emission shows one broad band centered at ~400 nm that tails into the visible and supports our assignment that these two emissions share separate electronic origins. We suspect that this emission arises from the T^{3+} species within the $T_7[PbBr_6]_3{\cdot}[Br]_9{\cdot}$DMF material as it shares similar emission characteristics to that T·3HBr. Both features display fast recombination dynamics with lifetimes of <1, 1.8, 8.1 ns for the 404 nm band and <1, 1.5, 4.4 ns for the 520 nm band (the first component is IRF limited and cannot be further determined).

The luminescence properties of the 0D tin compound, $T_2Sn_3Br_{18}{\cdot}4H_2O{\cdot}0.5Br_2$, are presented detailed in the Supporting Information (**Figure S10**). This compound displays a single very broad luminescence feature centered at ~710 nm with a FWHM of 200 nm. This emission is long-lived and shows triexponential decay dynamics with lifetimes of 2.2 ns, 138 ns, and 1.4 μs, with an average decay time of 1.2 μs. The excitation spectrum corresponding to this emission shows a strong feature at ~350 nm that is consistent with absorption in isolated $[SnBr_6]^{2-}$ octahedra.[109] Based on the breadth and long lifetime of this feature, we assign it to self-trapped excitonic emission, which is further consistent with reports of luminescence in the 0D Cs_4SnBr_6 system.[109]

Valence Band Maximum (VBM) Energy:

Photoemission yield spectroscopy in air (PYSA) was utilized to measure the absolute VBM energy of the materials in order to derive the band energy diagrams of the studied materials (**Figure 8**).[110-111] The position of the VBM in the band energy diagrams was determined through the PYSA measurements, while the conduction band minimum (CBM) was determined by subtracting the corresponding band gap values (based on the absorption edge) from the measured VBM energies. The VBM of T·3HBr a smaller value of -5.77 in comparison to -5.57 of T. 0D compounds $T_7Pb_3Br_{27}{\cdot}$DMF and $T_2Sn_3Br_{18}{\cdot}4H_2O{\cdot}0.5Br_2$ have close VBM values of -5.64 and -5.55

respectively. Given the similar range in value of the VBM for $(T\text{-}Et_6)_3Pb_{11}I_{31}$ (-5.62) to the 0D compounds, the reduced bandgap of this cubic compound is a result of the lowest unoccupied molecular orbital (LUMO) of the component $(T\text{-}Et_6)^{3+}$ cations. Since the hydrogen bond donor amine-groups are electronically isolated from the aromatic moieties of the T-based molecules, the lower energy LUMO in $(T\text{-}Et_6)_3Pb_{11}I_{31}$ can be attributed to supramolecular effects.

Electronic Properties:

Rationalization of the electronic structure of $(T\text{-}Et_6)_3Pb_{11}I_{31}$ is provided by computational investigations based on density functional theory (DFT, see **S.I.**). The large cubic crystal structure, with unit cell dimension greater than 30 Å, is considered using the corresponding primitive cell in which the entangled $[Pb_{11}I_{31}]^{9-}$ chains are now along (1,0,0), (0,1,0), (0,0,1) and (1,1,1), and that counts half the number of atoms. However, the resulting simulation cell remains too large (1212 atoms) to allow treatments beyond plain DFT, such as hybrid functionals, that would offer, for instance, a better description of the material's band gap.

The calculated band structure of $(T\text{-}Et_6)_3Pb_{11}I_{31}$ (**Figure 9A**) shows a band gap of 2.27 eV and essentially flat bands around the Fermi level with bandwidths of the order of 1 meV (**Figure S12**). Such a low dispersion, detrimental to charge carrier transport properties, can be expected when the corner-sharing connectivity of perovskites is substituted by face-sharing octahedra.[82] The valence band maximum (VBM, **Figure 9B**) is distributed over the inorganic chains and illustrates the three-fold symmetry imposed by the $Ia\bar{3}$ space group. On the other hand, the conduction band minimum (CBM, **Figure 9C**) involves the π-system of organic cations (**Figure S13**) and no visible contribution from the lead and iodide atoms. This is confirmed looking at the sharp peak of $(T\text{-}Et_6)$ states above the band gap in the projected density of states (pDOS, **Figure 9D** and **S14**). In addition, we observe that the VBM (**Figure 9B**) is formed by the contributions of the iodide dangling bonds found in the 6 edge-sharing octahedra cluster part of the inorganic network.

To explore further the electronic structure of $(T\text{-}Et_6)_3Pb_{11}I_{31}$, we carried out a crystal orbital Hamilton population (COHP) bonding analysis (**Figure 9E**).[112] We find a weak antibonding interactions between $[Pb_{11}I_{31}]^{9-}$ chains, that are less than 5 Å apart, close to the Fermi level. This coupling also appears when considering the band structures of a sub-network of 1D halide chains, that present strictly non-dispersive bands (**Figure S15**). Then, when we add the sub-networks of

1D halide chains one after the other, we can see the energy dispersion increase. More importantly, the COHP analysis shows a significant bonding interaction between the inorganic network and T-Et_6 cations that are in close contact with the $[Pb_{11}I_{31}]^{9-}$ chains (black line, **Figure 9E**). This strong coupling between the inorganic and organic moieties greatly affects the band structure and one can see that the cations tend to relocalize the valence states close to the Fermi level (**Figure S16**). Our computed bandgap (2.27 eV) is greater than the measured absorption edge (1.90 eV) and the low-temperature PL peak (1.65 eV). Since the GGA functional used here should lead to a significant bandgap underestimation, we can infer that the optical features cannot be assigned to band-to-band transitions but rather attributed the 0D character of the electronic density of states that may induce in turn a strong localization of excitonic resonance in the lattice.

Conclusions

Understanding how to acquire and tune novel structural motifs in functional hybrid materials with high structural complexity is necessary for predictive materials synthesis of well-defined structure-property relationships with technological relevance. The cubic lead halide frameworks of $(T\text{-}Et_6)_3Pb_{11}X_{31}$ (X=I, Br) based on the *C*$_3$-symmetric propeller-shaped triamine T: 1,3,5-tris-(4-aminophenyl)benzene form in ethanol by an efficient *in situ* N-diethylation and one-step reaction through solvothermal synthesis. These materials constitute a new structural class of hybrid lead halides with 3D topology. $(T\text{-}Et_6)_3Pb_{11}X_{31}$ (X=I, Br) consist of a unique structural motif of embedded $(T\text{-}Et_6)^{3+}$ cations and $[Pb_{11}X_{31}]^{9-}$ 1D chains composed of solely octahedral lead halide units with face- and edge-sharing connectivity. The octahedral lead halide subunits feature rare octahedral coordination environment of I5 and Br5 atoms within a Pb-X network with NaCl-type cell. The highly periodic structural class $(T\text{-}Et_6)_3Pb_{11}X_{31}$ expands current descriptive crystal chemistry with its homogenous cubic packing that can serve a basis for exploration of porous materials and for post-synthetic transformations in the solid state yielding multifunctional materials. The piece-by-piece electronic structure of $(T\text{-}Et_6)_3Pb_{11}I_{31}$ shows the weak interaction between chains, which eventually lead to flat valence bands because of the interaction between the chains and the organic cations from the conduction band. $(T\text{-}Et_6)_3Pb_{11}I_{31}$ exhibits an absorption onset at 1.72 eV with weak broad emission at centered at ~660 nm at 78K. In particular, the water stability of $(T\text{-}Et_6)_3Pb_{11}I_{31}$, due to the hydrophobic $(T\text{-}Et_6)^{3+}$ cations, initiates a new synthetic strategy in the rational design of environmentally robust hybrid halides. Additionally, the synthetic exploration of hybrid metal halides based on T^{3+} cations demonstrates adjustable structural

variations of 0D structures through ambient-pressure solution synthesis, ensuing compounds $T_7Pb_3Br_{27}$·DMF and $T_2Sn_3Br_{18}$·$4H_2O$·$0.5Br_2$. Despite their simple structural motifs of isolated [MX_6] octahedra (M=Pb^{2+}, Sn^{4+}) with T^{3+} cations in between, both $T_7Pb_3Br_{27}$·DMF and $T_2Sn_3Br_{18}$·$4H_2O$·$0.5Br_2$ feature blue PL emission at room temperature as a result of embodying luminophore T. This study introduces the fundamental structural design principles for creating novel, periodic hybrid materials using metal halide compounds that incorporate highly symmetric luminophores with enhanced moisture stability. The connectivity modes of the metal-halide octahedra can be directed through tuning the organic and inorganic components, thereby enabling the fine-tuning of the electronic structure and optoelectronic properties of the resulting materials.

Acknowledgments:

This work is supported by the U. S. Department of Energy, Office of Science, Basic Energy Sciences, under the grant DE-SC-0012541. E.S.V. acknowledges the Dr. John N. Nicholson fellowship through Northwestern University. A.K.I and M.G.K. would like to acknowledge the Air Force Office of Scientific Research Grant number FA9550-18-S-0003. I.S. acknowledges support from USF startup funds. J.L.F. was supported by an Arnold O. Beckman Postdoctoral Fellowship from the Arnold and Mabel Beckman Foundation (USA). This work made use of the NUANCE Center and IMSERC facilities of Northwestern University, which have received support from the Soft and Hybrid Nanotechnology Experimental (SHyNE) Resource (NSF ECCS-2025633). E.S.V. thanks Dr. Christos Malliakas, Prof. Ram Seshadri, Prof. Anthony Cheetham and Prof. Michael Chabinyc for productive discussion.

Associated Content:

Supporting Information

Methods, complementary syntheses, additional structural and characterization data: nanoindentation data, single crystal and powder X-ray diffraction, electronic structure and dielectric calculations, optical data, NMR spectroscopy, SEM and microscope images. This material is available free of charge via the Internet at http://pubs.acs.org.

X-ray crystallographic data for $(T\text{-}Et_6)_3Pb_{11}I_{31}$, CCDC 2216515

X-ray crystallographic data for $(T\text{-}Et_6)_3Pb_{11}Br_{31}$, CCDC 2216514

X-ray crystallographic data for $T_7Pb_3Br_{27}{\cdot}DMF$, CCDC 2216512

X-ray crystallographic data for $T_2Sn_3Br_{18}{\cdot}4H_2O{\cdot}0.5Br_2$, CCDC 2216513

Author Information:
Corresponding Authors
m-kanatzidis@northwestern.edu

Notes:

The authors declare no competing financial interest.

Figures:

Scheme 1. In situ N-Diethylation of T Luminophore

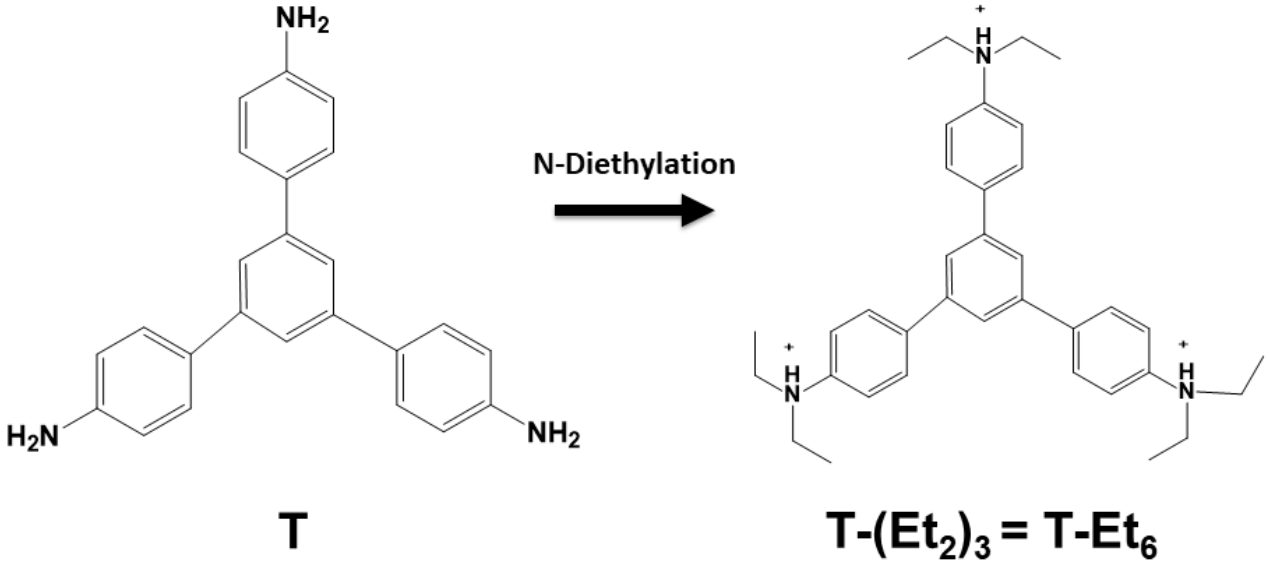

Table 1. Crystal Data and Structure Refinement for Novel $(T\text{-}Et_6)_3Pb_{11}X_{31}$ compounds

	$(T\text{-}Et_6)_3Pb_{11}I_{31}$	$(T\text{-}Et_6)_3Pb_{11}Br_{31}$
Empirical formula	$C_{108}H_{117}N_9Pb_{11}I_{31}$	$C_{108}H_{117}N_9Pb_{11}Br_{31}$
Crystal system	cubic	cubic
Space group	$Ia\bar{3}$	$Ia\bar{3}$
Crystal Shape and Color	Brown-Yellow Rod	Orange-Yellow Block
Unit cell dimensions (Å)	a = 32.78380(10)	a = 31.9220(2)
	α = β= γ=90°	α = β= γ=90°
Volume (Å^3)	35235.3 (3)	32529.0(6)
Z	8.00016	8.0016
Density (g/cm^3)	2.931	2.567
Independent reflections	8579 [R_{int} = 0.0459]	6710 [R_{int} = 0.0543]
Completeness to θ = 25.242°	99.9%	99.9%
Data k/ restraints / parameters	8579 / 7 / 204	6710 / 0 / 145
Goodness-of-fit	1.035	1.055
Final R indices [I>2σ(I)]	R_{obs} = 0.0494, wR_{obs} = 0.1235	R_{obs} = 0.0798, wR_{obs} = 0.2478
R indices [all data]	R_{all} = 0.0790, wR_{all} = 0.1394	R_{all} = 0.1366, wR_{all} = 0.2785

Table 2. Summary of structural parameters of novel $(T\text{-}Et_6)_3Pb_{11}X_{31}$ compounds

	$(T\text{-}Et_6)_3Pb_{11}I_{31}$	**$(T\text{-}Et_6)_3Pb_{11}Br_{31}$**
Average Pb-X Bond Length (Å)	3.213 Å	3.086 Å
Distance between 1D $[Pb_{11}X_{31}]^{9-}$ Chains (Å)	4.486 Å	4.852 Å
Angle between 1D $[Pb_{11}X_{31}]^{9-}$ Chains (°)	70.53 °	70.53 °

Table 3. Summary of optical properties of studied compounds

Compound	**Extrapolated Bandgap (eV)**	**VBM (eV)**	**CBM (eV)**
T	-	5.57	2.50
T·3HBr	2.24	5.77	2.40
$(T\text{-}Et_6)_3Pb_{11}I_{31}$	1.72	5.62	1.75
$T_7Pb_3Br_{27}$·DMF	2.75	5.64	2.20
$T_2Sn_3Br_{18}$·$4H_2O$·$0.5Br_2$	2.40	5.55	2.45

A

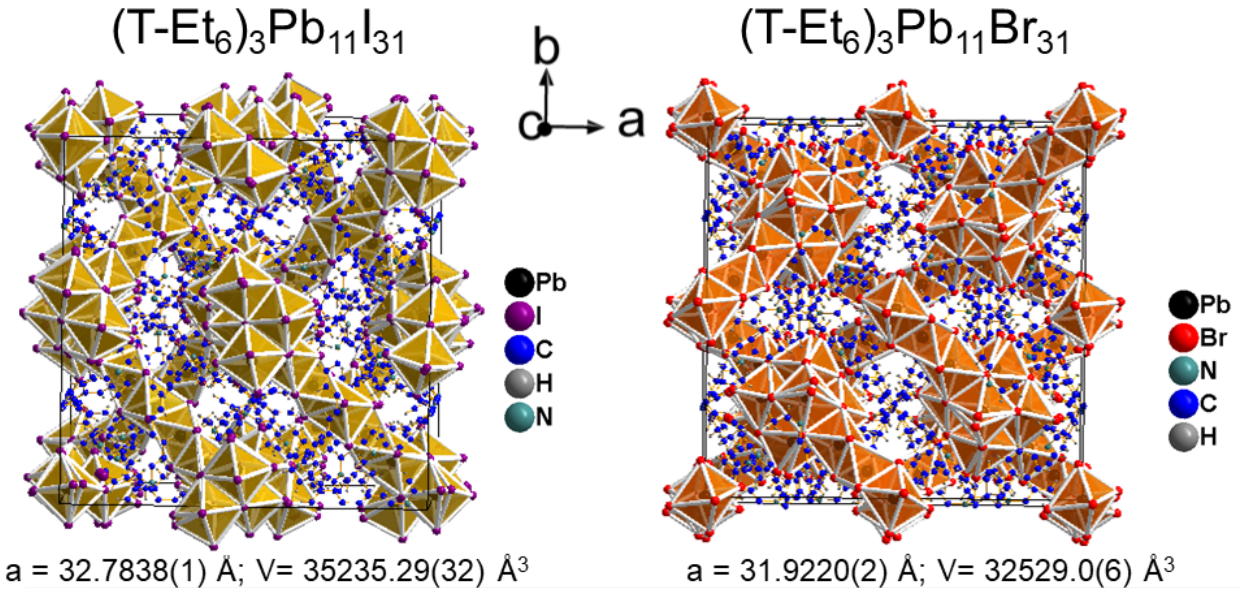
(T-Et6)3Pb11I31
b
c
a
Pb
I
C
H
N
(T-Et6)3Pb11Br31
Pb
Br
N
C
H
a = 32.7838(1) Å; V= 35235.29(32) Å3
a = 31.9220(2) Å; V= 32529.0(6) Å3

B

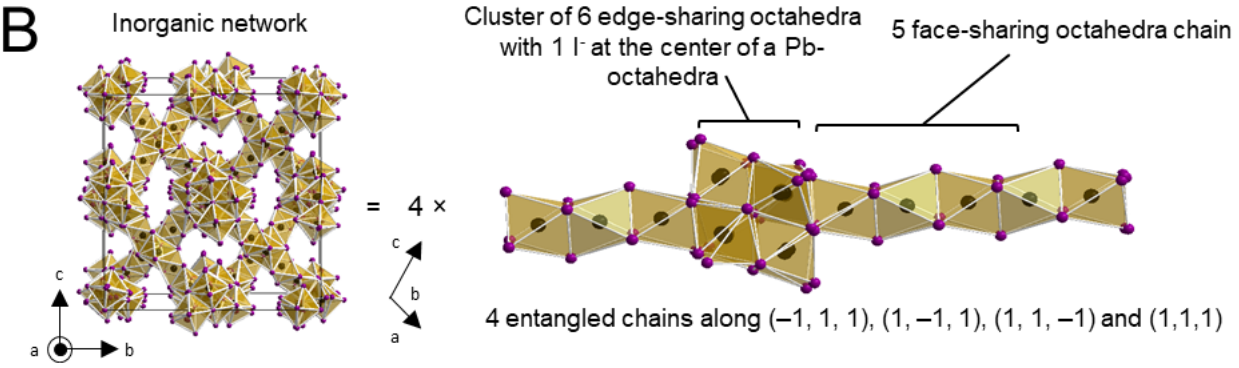
Inorganic network
= 4 ×
c
b
a
Cluster of 6 edge-sharing octahedra with 1 I- at the center of a Pb-octahedra
5 face-sharing octahedra chain
4 entangled chains along (–1, 1, 1), (1, –1, 1), (1, 1, –1) and (1,1,1)

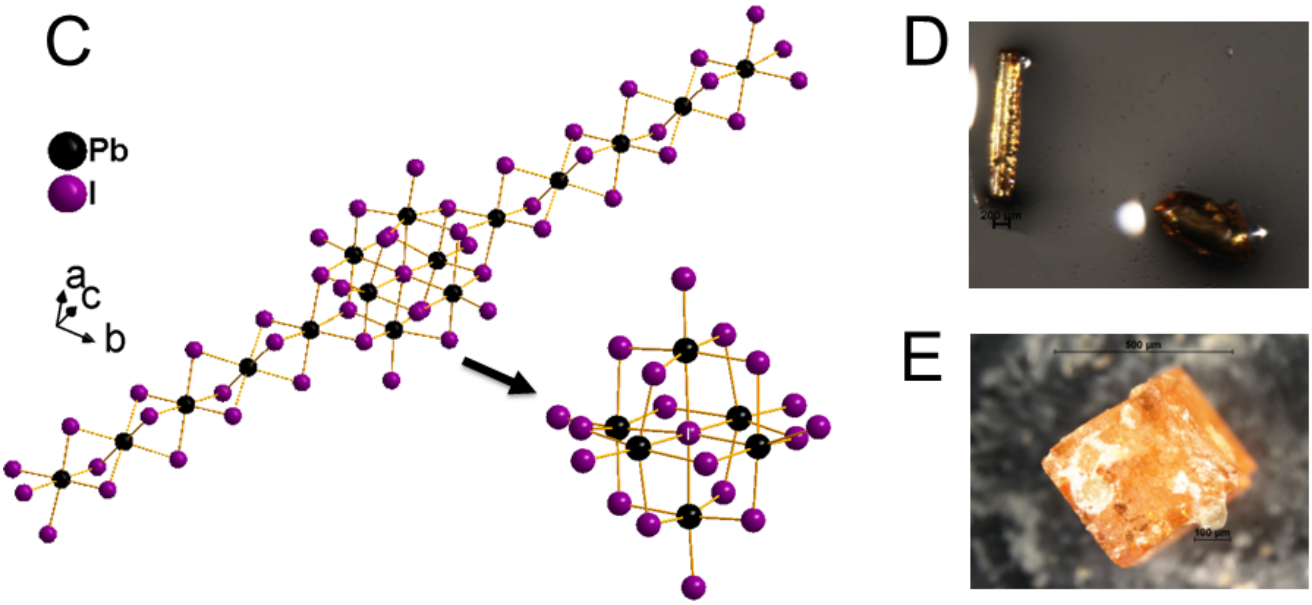

Figure 1. (A) Unit cell of crystal structures $(T\text{-}Et_6)_3Pb_{11}I_{31}$ and $(T\text{-}Et_6)_3Pb_{11}Br_{31}$ with 3D cubic topology viewed along the c-axis denoting the unit cell dimensions and volume respectively **(B)** Polyhedral view of $(T\text{-}Et_6)_3Pb_{11}I_{31}$ decompounded into its fundamental $[Pb_{11}I_{31}]^{9-}$ entanglement chain featuring 5 consecutive face-sharing $[PbI_6]^{4-}$ units connected to a cluster of 6 edge-sharing $[PbI_6]^{4-}$ units **(C)** View of repeating unit of $[Pb_{11}I_{31}]^{9-}$ chain highlighting the octahedral coordination environment of I5 atom within a NaCl-type $[Pb_6I_{19}]$ cluster along the ab plane **(D)** Microscope image of $(T\text{-}Et_6)_3Pb_{11}I_{31}$ crystal **(E)** Microscope image of $(T\text{-}Et_6)_3Pb_{11}Br_{31}$ crystal.

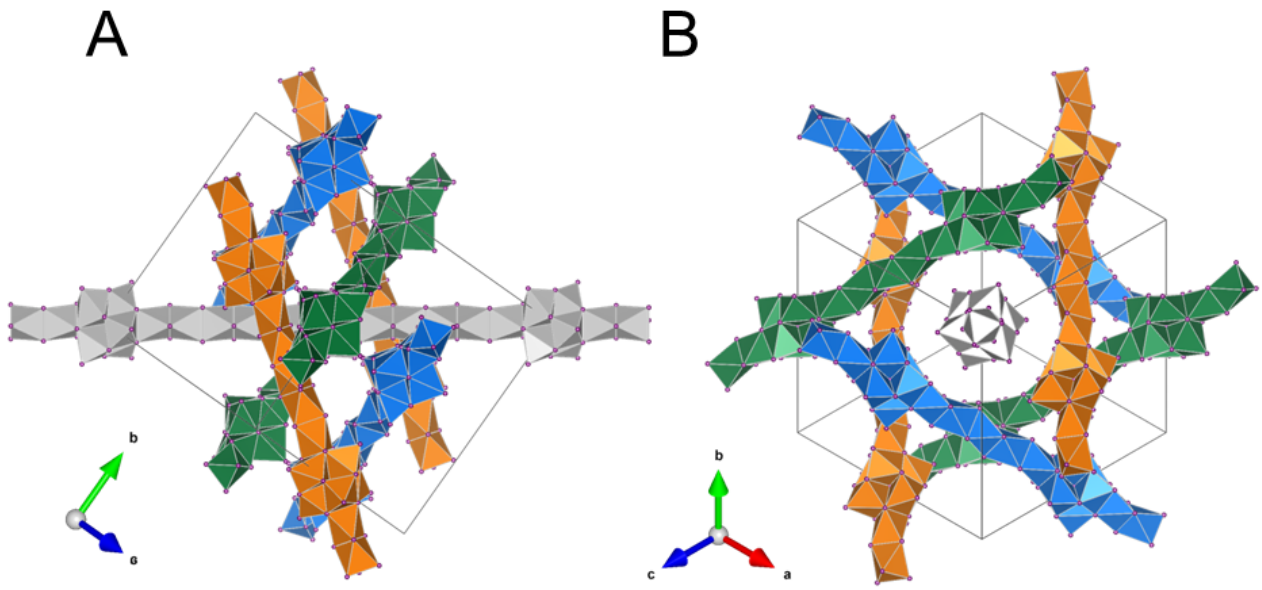

Figure 2. View of the different orientations of the distinct 1D $[Pb_{11}I_{31}]^{9-}$ entanglement chains in the $(T\text{-}Et_6)_3Pb_{11}I_{31}$ unit cell where the organic cations have been omitted in the depiction. The 1D $[Pb_{11}I_{31}]^{9-}$ chains with the same color are directed in the same orientation. **(A)** View from [100] direction. Altogether the entanglement of the 1D $[Pb_{11}I_{31}]^{9-}$ chains gives rise to the 3D topology of compound $(T\text{-}Et_6)_3Pb_{11}I_{31}$. **(B)** View along the [111] direction where the distance between two distinct chains is 4.486 Å and the angle between the chains is 70.53°.

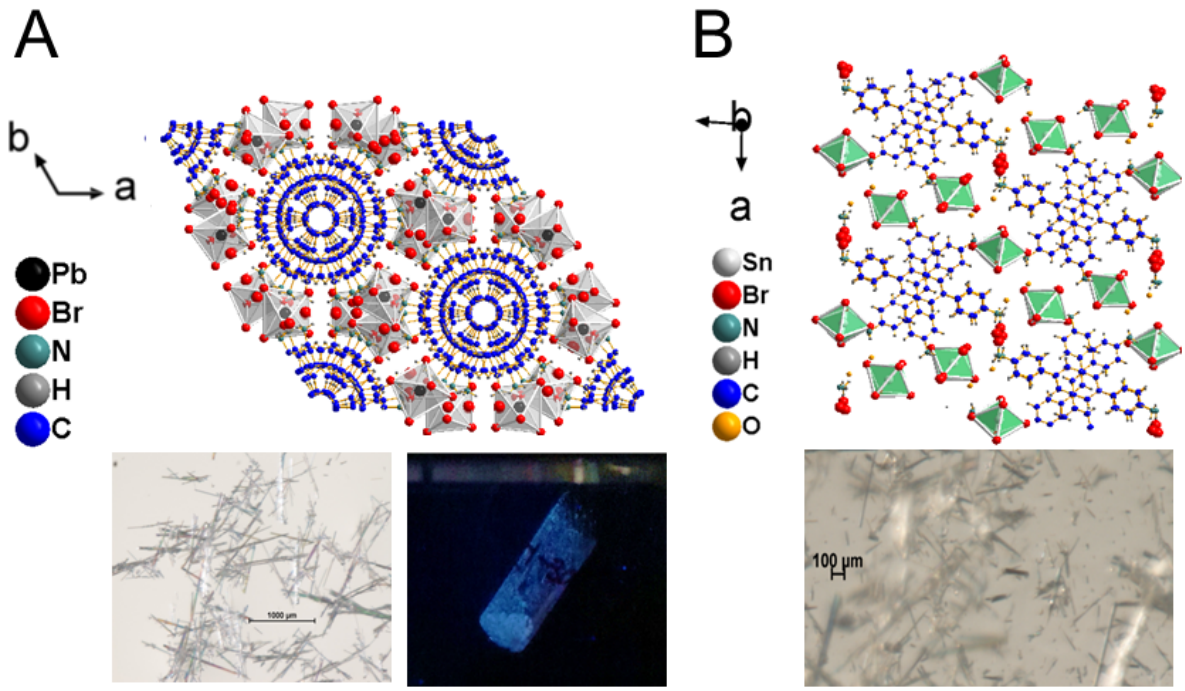

Figure 3. Crystal structure of 0D structures obtained through solution synthesis at ambient-pressure along with microscope image of crystals **(A)** $T_7Pb_3Br_{27}{\cdot}DMF$ that belongs to *R*-3*c* space group with unit cell dimensions a = b = 29.014(2) Å, c = 34.682(4) Å and γ = 120°. Microscope image of $T_7Pb_3Br_{27}{\cdot}DMF$ crystals, followed by picture of vial of dried $T_7Pb_3Br_{27}{\cdot}DMF$ crystalline powder under UV illumination in the dark. **(B)** $T_2Sn_3Br_{18}{\cdot}4H_2O{\cdot}0.5Br_2$ that belongs to $P2_1/n$ space group with unit cell dimensions a = 17.436(15) Å, b = 7.362(6) Å, c = 30.01(3) Å and β = 94.163(10)°.

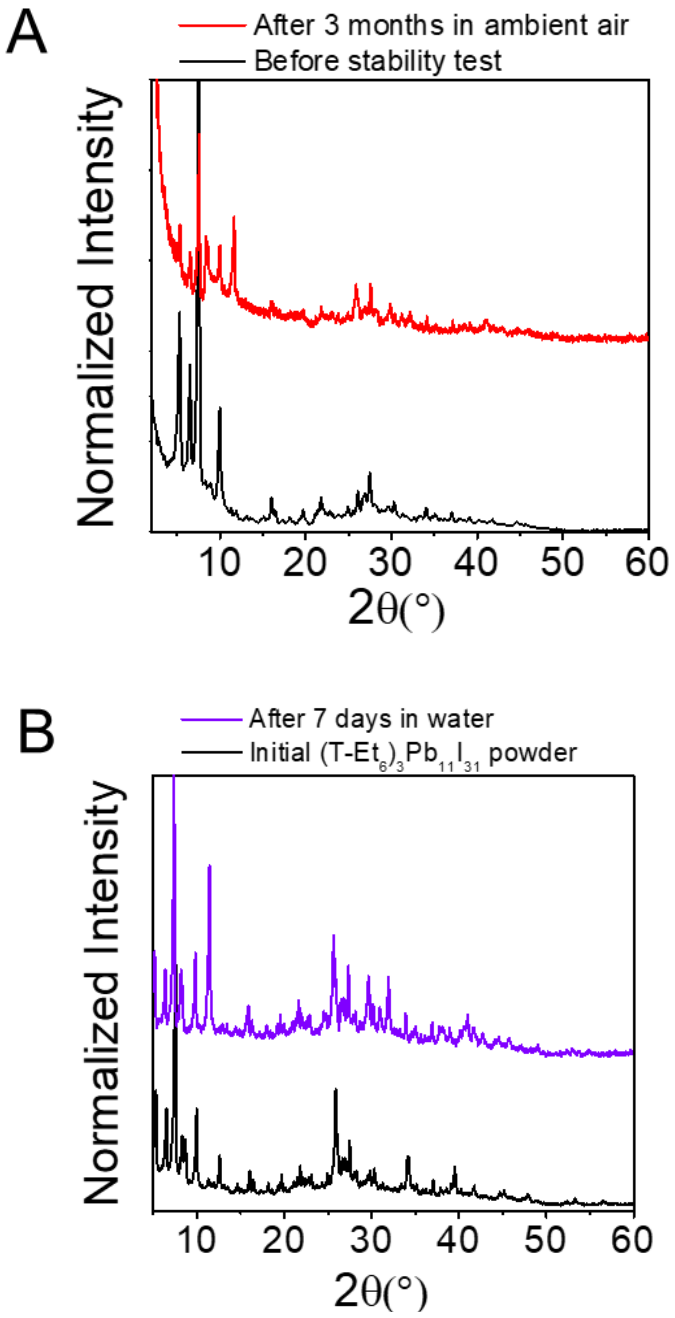

Figure 4. (A) PXRD pattern of $(T\text{-}Et_6)_3Pb_{11}I_{31}$ crystals before and after 3 months stored in ambient air. **(B)** PXRD pattern of $(T\text{-}Et_6)_3Pb_{11}I_{31}$ crystals before and after 7 days in water.

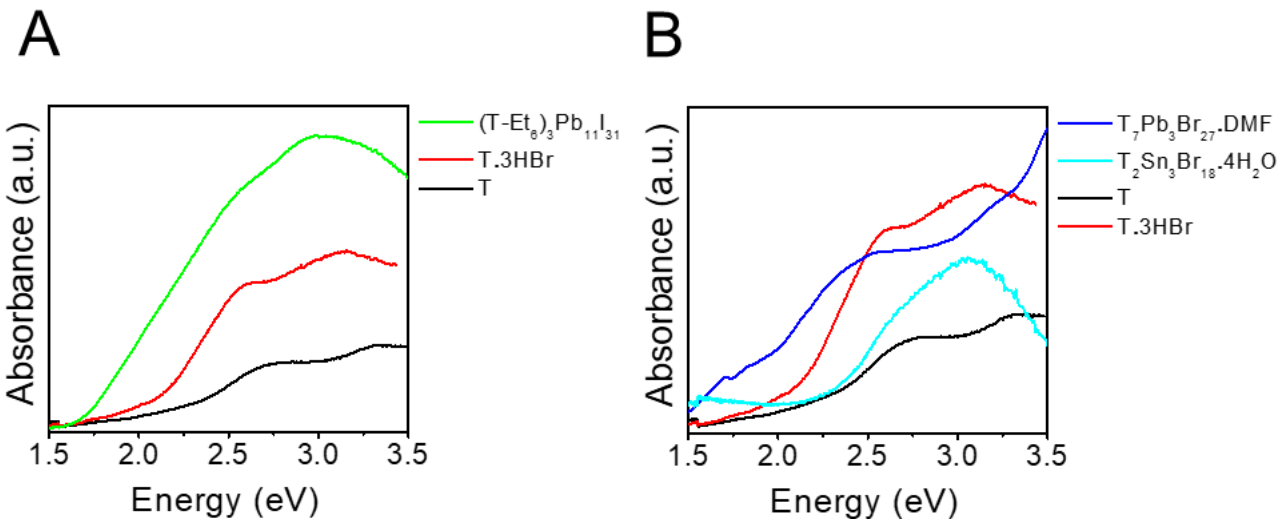

Figure 5. Solid-state optical absorption spectra of compounds **(A)** $(T\text{-}Et_6)_3Pb_{11}I_{31}$ alongside T and T·3HBr, **(B)** $T_7Pb_3Br_{27}$·DMF and $T_2Sn_3Br_{18}$·$4H_2O$·$0.5Br_2$ alongside T and T·3HBr.

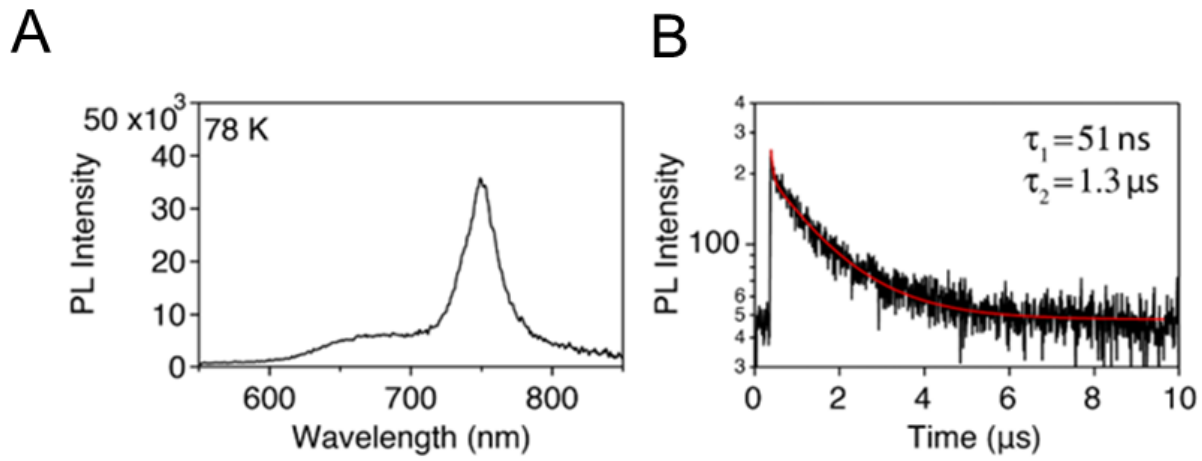

Figure 6. Steady-state PL emission spectrum for $(T\text{-}Et_6)_3Pb_{11}I_{31}$ at 78 K **(A)** followed by the time-resolved PL dynamics at 78 K **(B)**. The compound shows biexponential recovery dynamics with lifetimes of 51 ns and 1.3 µs.

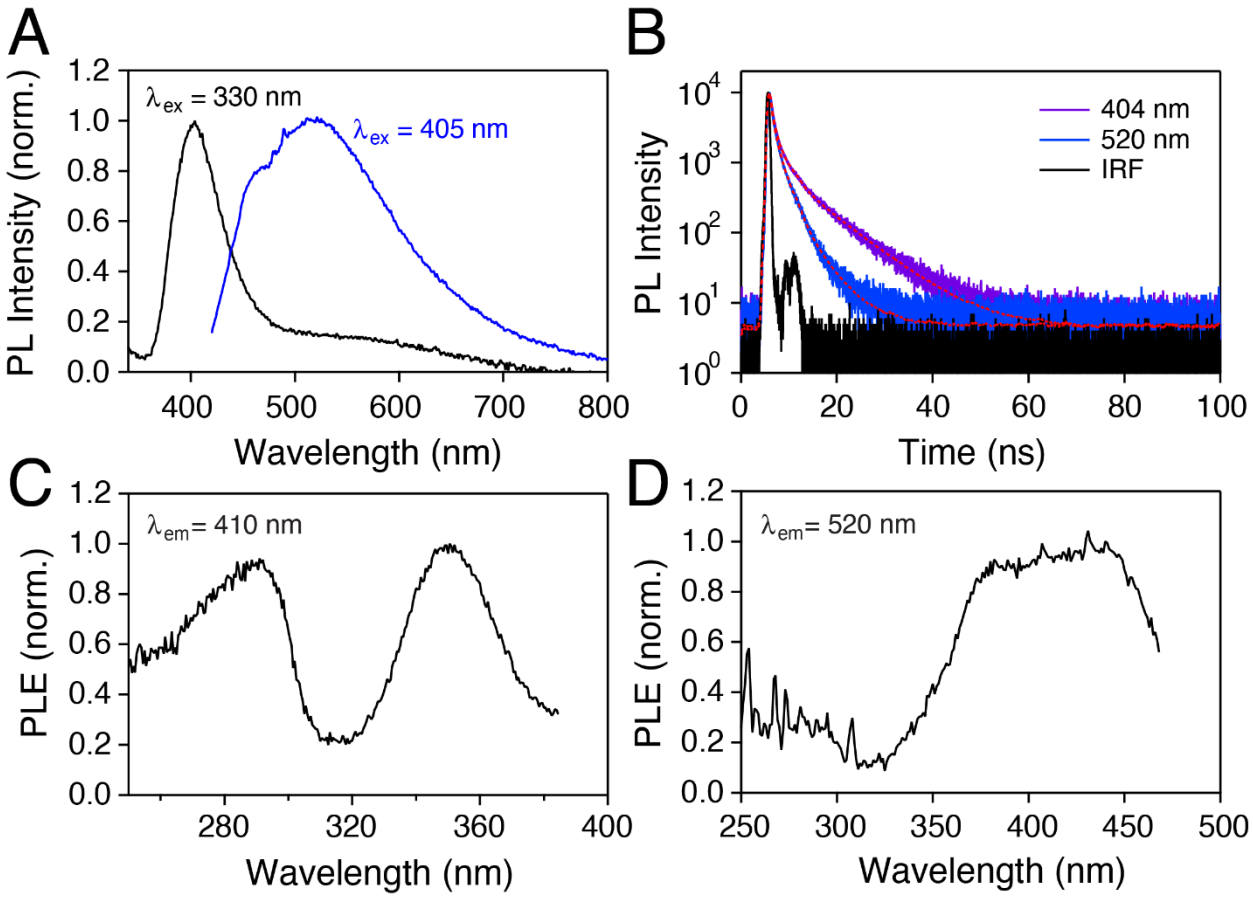

Figure 7. Steady-state and time-resolved PL emission and excitation spectra for $T_7Pb_3Br_{27}$·DMF. **(A)** gives the room-temperature PL spectra for $T_7Pb_3Br_{27}$·DMF when excited at 330 and 405 nm. Two distinct emission bands are observed depending on excitation wavelength. **(B)** The time-resolved PL for the two bands is fitted to a triexponential (red dash line) with lifetimes of <1, 1.8, 8.1 ns for the 404 nm band and <1, 1.5, 4.4 ns for the 520 nm band. The fast component is IRF limited. The photoluminescence excitation spectra for the emission at 410 nm **(C)** and 520 nm **(D)** show distinct differences consistent with these two emission bands sharing separate origins.

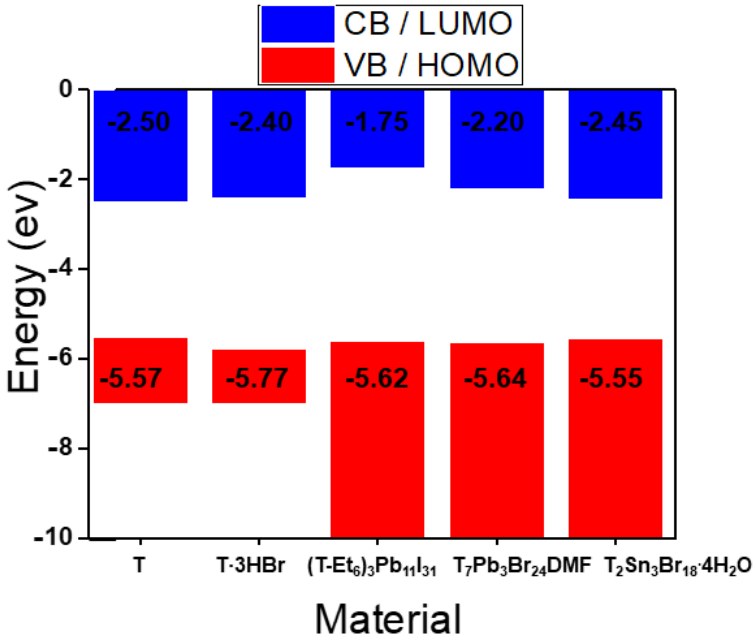

Figure 8. Band alignment diagram with valence band maximum energies determined from Photoemission Yield Spectroscopy in Air (PYSA) measurements of T, T·3HBr, 3D $(T\text{-}Et_6)_3Pb_{11}I_{31}$, 0D $T_7Pb_3Br_{27}$·DMF and 0D $T_2Sn_3Br_{18}{\cdot}4H_2O{\cdot}0.5Br_2$.

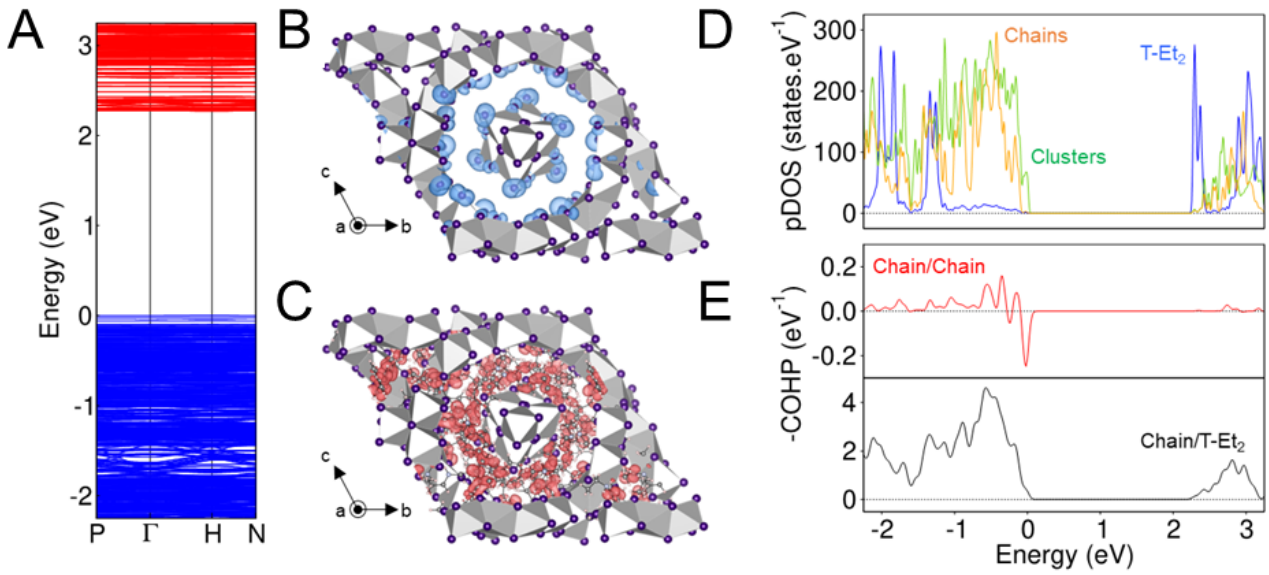

Figure 9. (A) DFT computed band structures of $(T\text{-}Et_6)_3Pb_{11}I_{31}$. **(B)** and **(C)** Partial charge densities taken at the valence band maximum (VBM, blue) and the conduction band minimum (CBM, red), respectively. For clarity, T-Et_6 cations are not depicted for the VBM that is distributed over $[Pb_{11}I_{31}]^{9-}$ chains, while the CBM is composed by contributions of the T-Et_6 cations. Identical

images would be obtained looking along the other chain directions, i.e. (0,1,0), (0,0,1) and (1,1,1). **(D)** Density of states projected over T-Et_6 cations (blue), the 5 face-sharing octahedra chain (orange) and the 6 edge-sharing octahedra cluster (green). **(E)** Crystal orbital Hamilton population (COHP) bonding analysis showing a week interaction between chains (red) and a strong interaction between the chains and the T-Et_6 cations. Bonding and anti-bonding interactions are represented by positive and negative values, respectively.

References:

1. Kojima, A.; Teshima, K.; Shirai, Y.; Miyasaka, T., Organometal Halide Perovskites as Visible-Light Sensitizers for Photovoltaic Cells. *J. Am. Chem. Soc.* **2009,** *131* (17), 6050-6051.
2. Chung, I.; Lee, B.; He, J.; Chang, R. P. H.; Kanatzidis, M. G., All-solid-state dye-sensitized solar cells with high efficiency. *Nature* **2012,** *485* (7399), 486-489.
3. Kim, H.-S.; Lee, C.-R.; Im, J.-H.; Lee, K.-B.; Moehl, T.; Marchioro, A.; Moon, S.-J.; Humphry-Baker, R.; Yum, J.-H.; Moser, J. E.; Grätzel, M.; Park, N.-G., Lead Iodide Perovskite Sensitized All-Solid-State Submicron Thin Film Mesoscopic Solar Cell with Efficiency Exceeding 9%. *Scientific Reports* **2012,** *2* (1), 591.
4. Lee, M. M.; Teuscher, J.; Miyasaka, T.; Murakami, T. N.; Snaith, H. J., Efficient Hybrid Solar Cells Based on Meso-Superstructured Organometal Halide Perovskites. *Science* **2012,** *338* (6107), 643.
5. Stoumpos, C. C.; Kanatzidis, M. G., Halide Perovskites: Poor Man's High-Performance Semiconductors. *Adv. Mater* **2016,** *28* (28), 5778-5793.
6. Tsai, H.; Nie, W.; Blancon, J.-C.; Stoumpos, C. C.; Asadpour, R.; Harutyunyan, B.; Neukirch, A. J.; Verduzco, R.; Crochet, J. J.; Tretiak, S.; Pedesseau, L.; Even, J.; Alam, M. A.; Gupta, G.; Lou, J.; Ajayan, P. M.; Bedzyk, M. J.; Kanatzidis, M. G.; Mohite, A. D., High-efficiency two-dimensional Ruddlesden–Popper perovskite solar cells. *Nature* **2016,** *536*, 312.
7. Arora, N.; Dar, M. I.; Hinderhofer, A.; Pellet, N.; Schreiber, F.; Zakeeruddin, S. M.; Grätzel, M., Perovskite solar cells with CuSCN hole extraction layers yield stabilized efficiencies greater than 20%. *Science* **2017,** *358* (6364), 768-771.
8. Yang, W. S.; Park, B.-W.; Jung, E. H.; Jeon, N. J.; Kim, Y. C.; Lee, D. U.; Shin, S. S.; Seo, J.; Kim, E. K.; Noh, J. H.; Seok, S. I., Iodide management in formamidinium-lead-halide–based perovskite layers for efficient solar cells. *Science* **2017,** *356* (6345), 1376-1379.
9. Tsai, H.; Asadpour, R.; Blancon, J.-C.; Stoumpos, C. C.; Durand, O.; Strzalka, J. W.; Chen, B.; Verduzco, R.; Ajayan, P. M.; Tretiak, S.; Even, J.; Alam, M. A.; Kanatzidis, M. G.; Nie, W.; Mohite, A. D., Light-induced lattice expansion leads to high-efficiency perovskite solar cells. *Science* **2018,** *360* (6384), 67-70.
10. Cao, Y.; Wang, N.; Tian, H.; Guo, J.; Wei, Y.; Chen, H.; Miao, Y.; Zou, W.; Pan, K.; He, Y.; Cao, H.; Ke, Y.; Xu, M.; Wang, Y.; Yang, M.; Du, K.; Fu, Z.; Kong, D.; Dai, D.; Jin, Y.; Li, G.; Li, H.; Peng, Q.; Wang, J.; Huang, W., Perovskite light-emitting diodes based on spontaneously formed submicrometre-scale structures. *Nature* **2018,** *562* (7726), 249-253.
11. Lin, K.; Xing, J.; Quan, L. N.; de Arquer, F. P. G.; Gong, X.; Lu, J.; Xie, L.; Zhao, W.; Zhang, D.; Yan, C.; Li, W.; Liu, X.; Lu, Y.; Kirman, J.; Sargent, E. H.; Xiong, Q.; Wei, Z., Perovskite light-emitting diodes with external quantum efficiency exceeding 20 per cent. *Nature* **2018,** *562* (7726), 245-248.
12. Sutherland, B. R.; Sargent, E. H., Perovskite photonic sources. *Nat. Photonics* **2016,** *10*, 295.
13. Fang, Y.; Dong, Q.; Shao, Y.; Yuan, Y.; Huang, J., Highly narrowband perovskite single-crystal photodetectors enabled by surface-charge recombination. *Nat. Photonics* **2015,** *9* (10), 679-686.
14. Wei, H.; Fang, Y.; Mulligan, P.; Chuirazzi, W.; Fang, H.-H.; Wang, C.; Ecker, B. R.; Gao, Y.; Loi, M. A.; Cao, L.; Huang, J., Sensitive X-ray detectors made of methylammonium lead tribromide perovskite single crystals. *Nat. Photonics* **2016,** *10* (5), 333-339.
15. Wei, H.; DeSantis, D.; Wei, W.; Deng, Y.; Guo, D.; Savenije, T. J.; Cao, L.; Huang, J., Dopant compensation in alloyed CH3NH3PbBr3−xClx perovskite single crystals for gamma-ray spectroscopy. *Nature Materials* **2017,** *16* (8), 826-833.
16. He, Y.; Ke, W.; Alexander, G. C. B.; McCall, K. M.; Chica, D. G.; Liu, Z.; Hadar, I.; Stoumpos, C. C.; Wessels, B. W.; Kanatzidis, M. G., Resolving the Energy of γ-Ray Photons with MAPbI3 Single Crystals. *ACS Photonics* **2018,** *5* (10), 4132-4138.

17. He, Y.; Matei, L.; Jung, H. J.; McCall, K. M.; Chen, M.; Stoumpos, C. C.; Liu, Z.; Peters, J. A.; Chung, D. Y.; Wessels, B. W.; Wasielewski, M. R.; Dravid, V. P.; Burger, A.; Kanatzidis, M. G., High spectral resolution of gamma-rays at room temperature by perovskite CsPbBr3 single crystals. *Nature Communications* **2018,** *9* (1), 1609.
18. Zhu, H.; Fu, Y.; Meng, F.; Wu, X.; Gong, Z.; Ding, Q.; Gustafsson, M. V.; Trinh, M. T.; Jin, S.; Zhu, X. Y., Lead halide perovskite nanowire lasers with low lasing thresholds and high quality factors. *Nature Materials* **2015,** *14* (6), 636-642.
19. Zhang, H.; Liao, Q.; Wu, Y.; Zhang, Z.; Gao, Q.; Liu, P.; Li, M.; Yao, J.; Fu, H., 2D Ruddlesden–Popper Perovskites Microring Laser Array. *Adv. Mater* **2018,** *30* (15), 1706186.
20. Mączka, M.; Gagor, A.; Zaręba, J. K.; Stefanska, D.; Drozd, M.; Balciunas, S.; Šimėnas, M.; Banys, J.; Sieradzki, A., Three-Dimensional Perovskite Methylhydrazinium Lead Chloride with Two Polar Phases and Unusual Second-Harmonic Generation Bistability above Room Temperature. *Chem. Mater.* **2020,** *32* (9), 4072-4082.
21. Mączka, M. a.; Ptak, M.; Gągor, A.; Stefańska, D.; Zaręba, J. K.; Sieradzki, A., Methylhydrazinium Lead Bromide: Noncentrosymmetric Three-Dimensional Perovskite with Exceptionally Large Framework Distortion and Green Photoluminescence. *Chem. Mater.* **2020,** *32* (4), 1667-1673.
22. Petrosova, H. R.; Kucheriv, O. I.; Shova, S.; Gural'skiy, I. A., Aziridinium cation templating 3D lead halide hybrid perovskites. *Chem Commun (Camb)* **2022,** *58* (38), 5745-5748.
23. Stoumpos, C. C.; Frazer, L.; Clark, D. J.; Kim, Y. S.; Rhim, S. H.; Freeman, A. J.; Ketterson, J. B.; Jang, J. I.; Kanatzidis, M. G., Hybrid Germanium Iodide Perovskite Semiconductors: Active Lone Pairs, Structural Distortions, Direct and Indirect Energy Gaps, and Strong Nonlinear Optical Properties. *J. Am. Chem. Soc.* **2015,** *137* (21), 6804-6819.
24. Dieter, W., CH3NH3PbX3, ein Pb(II)-System mit kubischer Perowskitstruktur / CH3NH3PbX3, a Pb(II)-System with Cubic Perovskite Structure. *Zeitschrift für Naturforschung B* **1978,** *33* (12), 1443-1445.
25. Goldschmidt, V. M., Die Gesetze der Krystallochemie. *Naturwissenschaften* **1926,** *14* (21), 477-485.
26. Niu, G.; Guo, X.; Wang, L., Review of recent progress in chemical stability of perovskite solar cells. *J. Mater. Chem. A* **2015,** *3* (17), 8970-8980.
27. Nagabhushana, G. P.; Shivaramaiah, R.; Navrotsky, A., Direct calorimetric verification of thermodynamic instability of lead halide hybrid perovskites. *Proc. Natl. Acad. Sci. U.S.A* **2016,** *113* (28), 7717-7721.
28. Spanopoulos, I.; Ke, W.; Kanatzidis, M. G., In Quest of Environmentally Stable Perovskite Solar Cells: A Perspective. *Helvetica Chimica Acta* **2020,** *104* (1), e2000173.
29. Vasileiadou, E. S.; Wang, B.; Spanopoulos, I.; Hadar, I.; Navrotsky, A.; Kanatzidis, M. G., Insight on the Stability of Thick Layers in 2D Ruddlesden–Popper and Dion–Jacobson Lead Iodide Perovskites. *J. Am. Chem. Soc.* **2021,** *143* (6), 2523-2536.
30. Cheng, S.; Zhong, H., What Happens When Halide Perovskites Meet with Water? *The Journal of Physical Chemistry Letters* **2022**, 2281-2290.
31. Raval, P.; Kennard, R. M.; Vasileiadou, E. S.; Dahlman, C. J.; Spanopoulos, I.; Chabinyc, M. L.; Kanatzidis, M.; Manjunatha Reddy, G. N., Understanding Instability in Formamidinium Lead Halide Perovskites: Kinetics of Transformative Reactions at Grain and Subgrain Boundaries. *ACS Energy Lett.* **2022**, 1534-1543.
32. Jayanthi, K.; Spanopoulos, I.; Zibouche, N.; Voskanyan, A. A.; Vasileiadou, E. S.; Islam, M. S.; Navrotsky, A.; Kanatzidis, M. G., Entropy Stabilization Effects and Ion Migration in 3D "Hollow" Halide Perovskites. *J. Am. Chem. Soc.* **2022,** *144* (18), 8223-8230.
33. Poglitsch, A.; Weber, D., Dynamic disorder in methylammoniumtrihalogenoplumbates (II) observed by millimeter-wave spectroscopy. *The Journal of Chemical Physics* **1987,** *87* (11), 6373-6378.

34. Swainson, I. P.; Hammond, R. P.; Soullière, C.; Knop, O.; Massa, W., Phase transitions in the perovskite methylammonium lead bromide, CH3ND3PbBr3. *Journal of Solid State Chemistry* **2003,** *176* (1), 97-104.
35. Stoumpos, C. C.; Malliakas, C. D.; Kanatzidis, M. G., Semiconducting Tin and Lead Iodide Perovskites with Organic Cations: Phase Transitions, High Mobilities, and Near-Infrared Photoluminescent Properties. *Inorg. Chem.* **2013,** *52* (15), 9019-9038.
36. Even, J.; Pedesseau, L.; Jancu, J.-M.; Katan, C., DFT and k · p modelling of the phase transitions of lead and tin halide perovskites for photovoltaic cells. *physica status solidi (RRL) – Rapid Research Letters* **2014,** *8* (1), 31-35.
37. Stoumpos, C. C.; Mao, L.; Malliakas, C. D.; Kanatzidis, M. G., Structure–Band Gap Relationships in Hexagonal Polytypes and Low-Dimensional Structures of Hybrid Tin Iodide Perovskites. *Inorg. Chem.* **2017,** *56* (1), 56-73.
38. Li, X.; He, Y.; Kepenekian, M.; Guo, P.; Ke, W.; Even, J.; Katan, C.; Stoumpos, C. C.; Schaller, R. D.; Kanatzidis, M. G., Three-Dimensional Lead Iodide Perovskitoid Hybrids with High X-ray Photoresponse. *J. Am. Chem. Soc.* **2020,** *142* (14), 6625-6637.
39. Tang, Y.-Y.; Liu, Y.-H.; Peng, H.; Deng, B.-B.; Cheng, T.-T.; Hu, Y.-T., Three-Dimensional Lead Bromide Hybrid Ferroelectric Realized by Lattice Expansion. *J. Am. Chem. Soc.* **2020,** *142* (46), 19698-19704.
40. Umeyama, D.; Leppert, L.; Connor, B. A.; Manumpil, M. A.; Neaton, J. B.; Karunadasa, H. I., Expanded Analogs of Three-Dimensional Lead-Halide Hybrid Perovskites. *Angew. Chem.* **2020,** *59* (43), 19087-19094.
41. Zhang, H.-Y.; Song, X.-J.; Cheng, H.; Zeng, Y.-L.; Zhang, Y.; Li, P.-F.; Liao, W.-Q.; Xiong, R.-G., A Three-Dimensional Lead Halide Perovskite-Related Ferroelectric. *J. Am. Chem. Soc.* **2020,** *142* (10), 4604-4608.
42. Li, X.; Kepenekian, M.; Li, L.; Dong, H.; Stoumpos, C. C.; Seshadri, R.; Katan, C.; Guo, P.; Even, J.; Kanatzidis, M. G., Tolerance Factor for Stabilizing 3D Hybrid Halide Perovskitoids Using Linear Diammonium Cations. *J. Am. Chem. Soc.* **2022,** *144* (9), 3902-3912.
43. Vasileiadou, E. S.; Jiang, X.; Kepenekian, M.; Even, J.; De Siena, M. C.; Klepov, V. V.; Friedrich, D.; Spanopoulos, I.; Tu, Q.; Tajuddin, I. S.; Weiss, E. A.; Kanatzidis, M. G., Thick-Layer Lead Iodide Perovskites with Bifunctional Organic Spacers Allylammonium and Iodopropylammonium Exhibiting Trap-State Emission. *J. Am. Chem. Soc.* **2022,** *144* (14), 6390-6409.
44. Matheu, R.; Ke, F.; Breidenbach, A.; Wolf, N.; Lee, Y.; Liu, Z.; Leppert, L.; Lin, Y.; Karunadasa, H., Charge Reservoirs in an Expanded Halide Perovskite Analog: Enhancing High-Pressure Conductivity through Redox-Active Molecules. *Angew. Chem. n/a* (n/a).
45. Fan, C.-C.; Liang, B.-D.; Liu, C.-D.; Chai, C.-Y.; Han, X.-B.; Zhang, W., Stable organic lead iodides with three-dimensional crystallographic and electronic structures showing high photoresponse. *Inorganic Chemistry Frontiers* **2022,** *9* (24), 6404-6411.
46. Zhang, Z.-J.; Xiang, S.-C.; Guo, G.-C.; Xu, G.; Wang, M.-S.; Zou, J.-P.; Guo, S.-P.; Huang, J.-S., Wavelength-Dependent Photochromic Inorganic–Organic Hybrid Based on a 3D Iodoplumbate Open-Framework Material. *Angew. Chem.* **2008,** *47* (22), 4149-4152.
47. Wang, G.-E.; Xu, G.; Wang, M.-S.; Cai, L.-Z.; Li, W.-H.; Guo, G.-C., Semiconductive 3-D haloplumbate framework hybrids with high color rendering index white-light emission. *Chem Sci* **2015,** *6* (12), 7222-7226.
48. Xie, G.; Wang, L.; Ju, D.; Yao, C.; Wang, X.; Song, S.; Qu, Y.; Li, H.; Tao, X., Thermochromism Perovskite (COOH(CH2)3NH3)2PbI4 Crystals: Single-Crystal to Single-Crystal Phase Transition and Excitation-Wavelength-Dependent Emission. *The Journal of Physical Chemistry Letters* **2022,** *13* (1), 214-221.

49. Stoumpos, C. C.; Cao, D. H.; Clark, D. J.; Young, J.; Rondinelli, J. M.; Jang, J. I.; Hupp, J. T.; Kanatzidis, M. G., Ruddlesden–Popper Hybrid Lead Iodide Perovskite 2D Homologous Semiconductors. *Chem. Mater.* **2016,** *28* (8), 2852-2867.
50. Smith, I. C.; Hoke, E. T.; Solis-Ibarra, D.; McGehee, M. D.; Karunadasa, H. I., A Layered Hybrid Perovskite Solar-Cell Absorber with Enhanced Moisture Stability. *Angew. Chem.* **2014,** *53* (42), 11232-11235.
51. Mao, L.; Ke, W.; Pedesseau, L.; Wu, Y.; Katan, C.; Even, J.; Wasielewski, M. R.; Stoumpos, C. C.; Kanatzidis, M. G., Hybrid Dion–Jacobson 2D Lead Iodide Perovskites. *J. Am. Chem. Soc.* **2018,** *140* (10), 3775-3783.
52. Vasileiadou, E. S.; Hadar, I.; Kepenekian, M.; Even, J.; Tu, Q.; Malliakas, C. D.; Friedrich, D.; Spanopoulos, I.; Hoffman, J. M.; Dravid, V. P.; Kanatzidis, M. G., Shedding Light on the Stability and Structure–Property Relationships of Two-Dimensional Hybrid Lead Bromide Perovskites. *Chem. Mater.* **2021,** *33* (13), 5085-5107.
53. Vasileiadou, E. S.; Kanatzidis, M. G., Structure-Property Relationships and Idiosyncrasies of Bulk, 2D Hybrid Lead Bromide Perovskites. *Israel Journal of Chemistry* **2021,** *61* (11-12), 782-817.
54. Li, X.; Hoffman, J. M.; Kanatzidis, M. G., The 2D Halide Perovskite Rulebook: How the Spacer Influences Everything from the Structure to Optoelectronic Device Efficiency. *Chem Rev* **2021,** *121* (4), 2230-2291.
55. Mączka, M.; Sobczak, S.; Ratajczyk, P.; Leite, F. F.; Paraguassu, W.; Dybała, F.; Herman, A. P.; Kudrawiec, R.; Katrusiak, A., Pressure-Driven Phase Transition in Two-Dimensional Perovskite MHy2PbBr4. *Chem. Mater.* **2022,** *34* (17), 7867-7877.
56. Spanopoulos, I.; Hadar, I.; Ke, W.; Guo, P.; Sidhik, S.; Kepenekian, M.; Even, J.; Mohite, A. D.; Schaller, R. D.; Kanatzidis, M. G., Water-Stable 1D Hybrid Tin(II) Iodide Emits Broad Light with 36% Photoluminescence Quantum Efficiency. *J Am Chem Soc* **2020,** *142* (19), 9028-9038.
57. Daub, M.; Hillebrecht, H., From 1D to 3D: Perovskites within the System HSC(NH(2))(2)I/CH(3)NH(3)I/PbI(2) with Maintenance of the Cubic Closest Packing. *Inorg Chem* **2021,** *60* (5), 3082-3093.
58. Yao, L.; Zeng, Z.; Cai, C.; Xu, P.; Gu, H.; Gao, L.; Han, J.; Zhang, X.; Wang, X.; Wang, X.; Pan, A.; Wang, J.; Liang, W.; Liu, S.; Chen, C.; Tang, J., Strong Second- and Third-Harmonic Generation in 1D Chiral Hybrid Bismuth Halides. *J Am Chem Soc* **2021,** *143* (39), 16095-16104.
59. Jiang, Y.; Fei, H., Efficient and Stable Self-Trapped Blue Emission from a 1D Organolead Chloride Crystalline Material. *Advanced Optical Materials* **2022,** *10* (5), 2102148.
60. Smółka, S.; Mączka, M.; Drozdowski, D.; Stefańska, D.; Gągor, A.; Sieradzki, A.; Zaręba, J. K.; Ptak, M., Effect of Dimensionality on Photoluminescence and Dielectric Properties of Imidazolium Lead Bromides. *Inorg. Chem.* **2022,** *61* (38), 15225-15238.
61. Zhou, C.; Tian, Y.; Wang, M.; Rose, A.; Besara, T.; Doyle, N. K.; Yuan, Z.; Wang, J. C.; Clark, R.; Hu, Y.; Siegrist, T.; Lin, S.; Ma, B., Low-Dimensional Organic Tin Bromide Perovskites and Their Photoinduced Structural Transformation. *Angew. Chem.* **2017,** *56* (31), 9018-9022.
62. Han, D.; Shi, H.; Ming, W.; Zhou, C.; Ma, B.; Saparov, B.; Ma, Y.-Z.; Chen, S.; Du, M.-H., Unraveling luminescence mechanisms in zero-dimensional halide perovskites. *Journal of Materials Chemistry C* **2018,** *6* (24), 6398-6405.
63. Zhou, C.; Lin, H.; Tian, Y.; Yuan, Z.; Clark, R.; Chen, B.; van de Burgt, L. J.; Wang, J. C.; Zhou, Y.; Hanson, K.; Meisner, Q. J.; Neu, J.; Besara, T.; Siegrist, T.; Lambers, E.; Djurovich, P.; Ma, B., Luminescent zero-dimensional organic metal halide hybrids with near-unity quantum efficiency. *Chem Sci* **2018,** *9* (3), 586-593.
64. Xu, L.-J.; Lin, H.; Lee, S.; Zhou, C.; Worku, M.; Chaaban, M.; He, Q.; Plaviak, A.; Lin, X.; Chen, B.; Du, M.-H.; Ma, B., 0D and 2D: The Cases of Phenylethylammonium Tin Bromide Hybrids. *Chem. Mater.* **2020,** *32* (11), 4692-4698.

65. Morad, V.; Shynkarenko, Y.; Yakunin, S.; Brumberg, A.; Schaller, R. D.; Kovalenko, M. V., Disphenoidal Zero-Dimensional Lead, Tin, and Germanium Halides: Highly Emissive Singlet and Triplet Self-Trapped Excitons and X-ray Scintillation. *J. Am. Chem. Soc.* **2019,** *141* (25), 9764-9768.
66. Passarelli, J. V.; Fairfield, D. J.; Sather, N. A.; Hendricks, M. P.; Sai, H.; Stern, C. L.; Stupp, S. I., Enhanced Out-of-Plane Conductivity and Photovoltaic Performance in n = 1 Layered Perovskites through Organic Cation Design. *J. Am. Chem. Soc.* **2018,** *140* (23), 7313-7323.
67. Benin, B. M.; Dirin, D. N.; Morad, V.; Wörle, M.; Yakunin, S.; Rainò, G.; Nazarenko, O.; Fischer, M.; Infante, I.; Kovalenko, M. V., Highly Emissive Self-Trapped Excitons in Fully Inorganic Zero-Dimensional Tin Halides. *Angew. Chem.* **2018,** *57* (35), 11329-11333.
68. Febriansyah, B.; Koh, T. M.; John, R. A.; Ganguly, R.; Li, Y.; Bruno, A.; Mhaisalkar, S. G.; England, J., Inducing Panchromatic Absorption and Photoconductivity in Polycrystalline Molecular 1D Lead-Iodide Perovskites through π-Stacked Viologens. *Chem. Mater.* **2018,** *30* (17), 5827-5830.
69. Spanopoulos, I.; Hadar, I.; Ke, W.; Guo, P.; Sidhik, S.; Kepenekian, M.; Even, J.; Mohite, A. D.; Schaller, R. D.; Kanatzidis, M. G., Water-Stable 1D Hybrid Tin(II) Iodide Emits Broad Light with 36% Photoluminescence Quantum Efficiency. *Journal of the American Chemical Society* **2020,** *142* (19), 9028-9038.
70. Tu, Q.; Spanopoulos, I.; Vasileiadou, E. S.; Li, X.; Kanatzidis, M. G.; Shekhawat, G. S.; Dravid, V. P., Exploring the Factors Affecting the Mechanical Properties of 2D Hybrid Organic-Inorganic Perovskites. *ACS Appl Mater Interfaces* **2020,** *12* (18), 20440-20447.
71. Daub, M.; Hillebrecht, H., From 1D to 3D: Perovskites within the System HSC(NH2)2I/CH3NH3I/PbI2 with Maintenance of the Cubic Closest Packing. *Inorganic Chemistry* **2021,** *60* (5), 3082-3093.
72. Kim, D.; Vasileiadou, E. S.; Spanopoulos, I.; Kanatzidis, M. G.; Tu, Q., In-Plane Mechanical Properties of Two-Dimensional Hybrid Organic–Inorganic Perovskite Nanosheets: Structure–Property Relationships. *ACS Appl. Mater. Interfaces* **2021,** *13* (27), 31642-31649.
73. Li, C.; Wang, K.; Li, X.-Y.; Jiang, X.-F.; Wei, Q.; Li, J.-H.; Wang, G.-M., Conjugated-Polypyridine-Derivative-Derived Semiconductive Iodoplumbates with Tunable Architectures and Efficient Visible-Light-Induced Photocatalytic Property. *Inorg. Chem.* **2021,** *60* (4), 2105-2111.
74. Panuganti, S.; Besteiro, L. V.; Vasileiadou, E. S.; Hoffman, J. M.; Govorov, A. O.; Gray, S. K.; Kanatzidis, M. G.; Schaller, R. D., Distance Dependence of Forster Resonance Energy Transfer Rates in 2D Perovskite Quantum Wells via Control of Organic Spacer Length. *J Am Chem Soc* **2021,** *143* (11), 4244-4252.
75. Song, G.; Li, Z.; Gong, P.; Xie, R.-J.; Lin, Z., Tunable White Light Emission in a Zero-Dimensional Organic–Inorganic Metal Halide Hybrid with Ultra-High Color Rendering Index. *Advanced Optical Materials* **2021,** *9* (11), 2002246.
76. Hoffman, J. M.; Hadar, I.; Li, X.; Ke, W.; Vasileiadou, E. S.; Strzalka, J.; Chen, L. X.; Kanatzidis, M. G., Film formation mechanisms in mixed-dimensional 2D/3D halide perovskite films revealed by in situ grazing-incidence wide-angle X-ray scattering. *Chem* **2022,** *8* (4), 1067-1082.
77. Mao, L.; Wu, Y.; Stoumpos, C. C.; Traore, B.; Katan, C.; Even, J.; Wasielewski, M. R.; Kanatzidis, M. G., Tunable White-Light Emission in Single-Cation-Templated Three-Layered 2D Perovskites (CH3CH2NH3)4Pb3Br10–xClx. *J. Am. Chem. Soc.* **2017,** *139* (34), 11956-11963.
78. Mao, L.; Wu, Y.; Stoumpos, C. C.; Wasielewski, M. R.; Kanatzidis, M. G., White-Light Emission and Structural Distortion in New Corrugated Two-Dimensional Lead Bromide Perovskites. *J. Am. Chem. Soc.* **2017,** *139* (14), 5210-5215.
79. Soe, C. M. M.; Stoumpos, C. C.; Kepenekian, M.; Traoré, B.; Tsai, H.; Nie, W.; Wang, B.; Katan, C.; Seshadri, R.; Mohite, A. D.; Even, J.; Marks, T. J.; Kanatzidis, M. G., New Type of 2D Perovskites with Alternating Cations in the Interlayer Space, (C(NH2)3)(CH3NH3)nPbnI3n+1: Structure, Properties, and Photovoltaic Performance. *J. Am. Chem. Soc.* **2017,** *139* (45), 16297-16309.

80. Li, X.; Hoffman, J.; Ke, W.; Chen, M.; Tsai, H.; Nie, W.; Mohite, A. D.; Kepenekian, M.; Katan, C.; Even, J.; Wasielewski, M. R.; Stoumpos, C. C.; Kanatzidis, M. G., Two-Dimensional Halide Perovskites Incorporating Straight Chain Symmetric Diammonium Ions, $(NH_3C_mH_{2m}NH_3)(CH_3NH_3)_{n-1}Pb_nI_{3n+1}$ (m = 4–9; n = 1–4). *J. Am. Chem. Soc.* **2018,** *140* (38), 12226-12238.
81. Mao, L.; Guo, P.; Kepenekian, M.; Hadar, I.; Katan, C.; Even, J.; Schaller, R. D.; Stoumpos, C. C.; Kanatzidis, M. G., Structural Diversity in White-Light-Emitting Hybrid Lead Bromide Perovskites. *J. Am. Chem. Soc.* **2018,** *140* (40), 13078-13088.
82. Hoffman, J. M.; Che, X.; Sidhik, S.; Li, X.; Hadar, I.; Blancon, J.-C.; Yamaguchi, H.; Kepenekian, M.; Katan, C.; Even, J.; Stoumpos, C. C.; Mohite, A. D.; Kanatzidis, M. G., From 2D to 1D Electronic Dimensionality in Halide Perovskites with Stepped and Flat Layers Using Propylammonium as a Spacer. *J. Am. Chem. Soc.* **2019,** *141* (27), 10661-10676.
83. Li, X.; Guo, P.; Kepenekian, M.; Hadar, I.; Katan, C.; Even, J.; Stoumpos, C. C.; Schaller, R. D.; Kanatzidis, M. G., Small Cyclic Diammonium Cation Templated (110)-Oriented 2D Halide (X = I, Br, Cl) Perovskites with White-Light Emission. *Chem. Mater.* **2019,** *31* (9), 3582-3590.
84. Li, X.; Ke, W.; Traoré, B.; Guo, P.; Hadar, I.; Kepenekian, M.; Even, J.; Katan, C.; Stoumpos, C. C.; Schaller, R. D.; Kanatzidis, M. G., Two-Dimensional Dion–Jacobson Hybrid Lead Iodide Perovskites with Aromatic Diammonium Cations. *J. Am. Chem. Soc.* **2019,** *141* (32), 12880-12890.
85. Spanopoulos, I.; Hadar, I.; Ke, W.; Tu, Q.; Chen, M.; Tsai, H.; He, Y.; Shekhawat, G.; Dravid, V. P.; Wasielewski, M. R.; Mohite, A. D.; Stoumpos, C. C.; Kanatzidis, M. G., Uniaxial Expansion of the 2D Ruddlesden–Popper Perovskite Family for Improved Environmental Stability. *J. Am. Chem. Soc.* **2019,** *141* (13), 5518-5534.
86. Hoffman, J. M.; Malliakas, C. D.; Sidhik, S.; Hadar, I.; McClain, R.; Mohite, A. D.; Kanatzidis, M. G., Long periodic ripple in a 2D hybrid halide perovskite structure using branched organic spacers. *Chem Sci* **2020,** *11* (44), 12139-12148.
87. Era, M.; Maeda, K.; Tsutsui, T., Enhanced phosphorescence from naphthalene-chromophore incorporated into lead bromide-based layered perovskite having organic–inorganic superlattice structure. *Chemical Physics Letters* **1998,** *296* (3), 417-420.
88. Braun, M.; Tuffentsammer, W.; Wachtel, H.; Wolf, H. C., Tailoring of energy levels in lead chloride based layered perovskites and energy transfer between the organic and inorganic planes. *Chemical Physics Letters* **1999,** *303* (1), 157-164.
89. Mitzi, D. B.; Chondroudis, K.; Kagan, C. R., Design, Structure, and Optical Properties of Organic–Inorganic Perovskites Containing an Oligothiophene Chromophore. *Inorg. Chem.* **1999,** *38* (26), 6246-6256.
90. Cortecchia, D.; Soci, C.; Cametti, M.; Petrozza, A.; Martí-Rujas, J., Crystal Engineering of a Two-Dimensional Lead-Free Perovskite with Functional Organic Cations by Second-Sphere Coordination. *ChemPlusChem* **2017,** *82* (5), 681-685.
91. Gao, Y.; Shi, E.; Deng, S.; Shiring, S. B.; Snaider, J. M.; Liang, C.; Yuan, B.; Song, R.; Janke, S. M.; Liebman-Peláez, A.; Yoo, P.; Zeller, M.; Boudouris, B. W.; Liao, P.; Zhu, C.; Blum, V.; Yu, Y.; Savoie, B. M.; Huang, L.; Dou, L., Molecular engineering of organic–inorganic hybrid perovskites quantum wells. *Nature Chemistry* **2019,** *11* (12), 1151-1157.
92. Leveillee, J.; Katan, C.; Even, J.; Ghosh, D.; Nie, W.; Mohite, A. D.; Tretiak, S.; Schleife, A.; Neukirch, A. J., Tuning Electronic Structure in Layered Hybrid Perovskites with Organic Spacer Substitution. *Nano Letters* **2019,** *19* (12), 8732-8740.
93. Sheikh, T.; Maqbool, S.; Mandal, P.; Nag, A., Introducing Intermolecular Cation-π Interactions for Water-Stable Low Dimensional Hybrid Lead Halide Perovskites. *Angew. Chem.* **2021,** *60* (33), 18265-18271.

94. Bartholomew, A. K.; Stone, I. B.; Steigerwald, M. L.; Lambert, T. H.; Roy, X., Highly Twisted Azobenzene Ligand Causes Crystals to Continuously Roll in Sunlight. *J. Am. Chem. Soc.* **2022,** *144* (37), 16773-16777.
95. Zhuang, Z.; Peng, C.; Zhang, G.; Yang, H.; Yin, J.; Fei, H., Intrinsic Broadband White-Light Emission from Ultrastable, Cationic Lead Halide Layered Materials. *Angewandte Chemie International Edition* **2017,** *56* (46), 14411-14416.
96. Xue, C.; Yao, Z.-Y.; Zhang, J.; Liu, W.-L.; Liu, J.-L.; Ren, X.-M., Extra thermo- and water-stable one-dimensional organic–inorganic hybrid perovskite [N-methyldabconium]PbI3 showing switchable dielectric behaviour, conductivity and bright yellow-green emission. *Chemical Communications* **2018,** *54* (34), 4321-4324.
97. Bhowal, R.; Balaraman, A. A.; Ghosh, M.; Dutta, S.; Dey, K. K.; Chopra, D., Probing Atomistic Behavior To Unravel Dielectric Phenomena in Charge Transfer Cocrystals. *J. Am. Chem. Soc.* **2021,** *143* (2), 1024-1037.
98. Mancini, A.; Quadrelli, P.; Amoroso, G.; Milanese, C.; Boiocchi, M.; Sironi, A.; Patrini, M.; Guizzetti, G.; Malavasi, L., Synthesis, structural and optical characterization of APbX3 (A=methylammonium, dimethylammonium, trimethylammonium; X=I, Br, Cl) hybrid organic-inorganic materials. *Journal of Solid State Chemistry* **2016,** *240*, 55-60.
99. Ke, W.; Spanopoulos, I.; Stoumpos, C. C.; Kanatzidis, M. G., Myths and reality of HPbI3 in halide perovskite solar cells. *Nature Communications* **2018,** *9* (1), 4785.
100. Li, W.; Wang, Z.; Deschler, F.; Gao, S.; Friend, R. H.; Cheetham, A. K., Chemically diverse and multifunctional hybrid organic–inorganic perovskites. *Nature Reviews Materials* **2017,** *2* (3), 16099.
101. O'Keeffe, M., Cubic cylinder packings. *Acta Crystallographica Section A* **1992,** *48* (6), 879-884.
102. O'Keeffe, M.; Plevert, J.; Ogawa, T., Homogeneous cubic cylinder packings revisited. *Acta Crystallographica Section A* **2002,** *58* (2), 125-132.
103. Tang, Z.; Guloy, A. M., A Methylviologen Lead(II) Iodide: Novel [PbI3-]∞ Chains with Mixed Octahedral and Trigonal Prismatic Coordination. *J. Am. Chem. Soc.* **1999,** *121* (2), 452-453.
104. Chen, Y.; Wang, Z.-O.; Yang, Z.; Ren, Z.-G.; Li, H.-X.; Lang, J.-P., Unique assembly of low-dimensional viologen iodoplumbates and their improved semiconducting properties. *Dalton Transactions* **2010,** *39* (40), 9476-9479.
105. Krautscheid, H.; Vielsack, F., [Pb18I44]8−−An Iodoplumbate with an Unusual Structure. *Angewandte Chemie International Edition in English* **1995,** *34* (18), 2035-2037.
106. Verbouwe, W.; Van der Auweraer, M.; De Schryver, F. C.; Piet, J. J.; Warman, J. M., Excited State Localization or Delocalization in C3-symmetric Amino-substituted Triphenylbenzene Derivatives. *J. Am. Chem. Soc.* **1998,** *120* (6), 1319-1324.
107. Yin, J.; Zhang, Y.; Bruno, A.; Soci, C.; Bakr, O. M.; Brédas, J.-L.; Mohammed, O. F., Intrinsic Lead Ion Emissions in Zero-Dimensional Cs4PbBr6 Nanocrystals. *ACS Energy Letters* **2017,** *2* (12), 2805-2811.
108. Petralanda, U.; Biffi, G.; Boehme, S. C.; Baranov, D.; Krahne, R.; Manna, L.; Infante, I., Fast Intrinsic Emission Quenching in Cs4PbBr6 Nanocrystals. *Nano Letters* **2021,** *21* (20), 8619-8626.
109. Zhang, X.; Wang, H.; Wang, S.; Hu, Y.; Liu, X.; Shi, Z.; Colvin, V. L.; Wang, S.; Yu, W. W.; Zhang, Y., Room Temperature Synthesis of All Inorganic Lead-Free Zero-Dimensional Cs4SnBr6 and Cs3KSnBr6 Perovskites. *Inorganic Chemistry* **2020,** *59* (1), 533-538.
110. Fujisawa, J.-i.; Ishihara, T., Charge-transfer transitions between wires and spacers in an inorganic-organic quasi-one-dimensional crystal methylviologen lead iodide. *Physical Review B* **2004,** *70* (11), 113203.
111. Harwell, J. R.; Baikie, T. K.; Baikie, I. D.; Payne, J. L.; Ni, C.; Irvine, J. T. S.; Turnbull, G. A.; Samuel, I. D. W., Probing the energy levels of perovskite solar cells via Kelvin probe and UV ambient pressure photoemission spectroscopy. *Physical Chemistry Chemical Physics* **2016,** *18* (29), 19738-19745.

112. Dronskowski, R.; Bloechl, P. E., Crystal orbital Hamilton populations (COHP): energy-resolved visualization of chemical bonding in solids based on density-functional calculations. *The Journal of Physical Chemistry* **1993,** *97* (33), 8617-8624.

Table of Contents